CHAPTER - III

LINEAR ALIPHATIC POLYESTERS AS CORROSION MITIGATORS FOR MILD STEEL IN 0.5 M H_2SO_4

3.1 INTRODUCTION

Metal dissolution is one of the major concern in recent days due to the usage of metals in various industrial sectors in acid influenced medium. It is a natural phenomenon which cannot be eliminated but can be controlled to an extent. Thus the protection of metallic structures against corrosion should be critically viewed. In order to overcome these issues socially and economically, the search towards efficient inhibitors has taken a new dimension. The consequences of corrosion are varied and the effects of these on the safe, reliable and efficient operation of equipment are often more serious than simple loss of a metal.

Industrial exercises like pickling, cleaning and descaling obviously generates lesser metal dissolution which could provide failure of machines and facilitates the necessity for new equipments[1]. Some of the hazardous effects of corrosion are,

(i) loss of technically important surface properties of metals

(ii) reduced value of goods due to deterioration of appearance

(iii) hazards or injuries to people arising from structural breakdown

(iv) corroded components to be replaced systematically

(v) mechanical damage by solid corrosion products

Virtually all corrosion reactions are spontaneous which can be minimised by employing suitable strategies which in turn stifle, retard or completely stop the corrosion process. The most applicable and possible method to control corrosion is by means of inhibitors.

Major class of corrosion inhibitors containing heteroatoms like N, O and S with multiple bonds fall under the class of organic compounds which has the capability of getting adsorbed onto the metal surface by adopting the following mechanisms[2],

(i) electrostatic attraction between charged molecule and the metal

(ii) interaction between the metal and uncharged electron pairs in the molecule

(iii) interaction between pi electron density and the metal.

(iv) combination of (i), (ii) and (iii).

The effectiveness of the organic inhibitors are related to their chemical composition, molecular structure and the affinity to get adsorbed on the mild steel surface. Since the whole idea of metal protection is anchored on economic gain, environmental sustainability and reaction feasibility, lot of research work is going on to synthesise an alternate material which is obviously a polymeric network, to replace high toxic and expensive organic inhibitors. The addition of high molecular weight[3] organic compounds such as polymer to inhibit corrosion finds a unique position due to its maximum solubility, evolution of less toxic gases, multi functionality and increased reactive sites.

Thus the present work has been framed to investigate the anticorrosive behaviour of linear aliphatic water soluble polyesters (synthesis described in chapter II) in 0.5 M H_2SO_4. As a correlation, knowledge about the previous work reported has been reviewed and summarised below.

3.1.1 Review of literature

Sabirneeza *et al.*, utilised FTIR, SEM - EDX and XRD techniques to characterise novel water soluble semiconducting polymer composite poly (vinyl alcohol–proline) (PVAP) and employed as corrosion inhibitor for mild steel in HCl medium. Influence of time, temperature and concentration were studied concluding with a report of highest inhibition efficiency of 94% for 0.6% (wt) at room temperature. Polarisation techniques revealed mixed type of inhibiton. Morphological examination also supported the same[4].

Rithin Kumar *et al.*, studied the influence of sulfonated polysulfone polymer (SPS) on mild steel corrosion in HCl medium with a result of 84% inhibition efficiency at 3000 ppm concentration. Increase in temperature favoured increased efficiency. The mode of adsorption was found to fit with Langmuir adsorption isotherm. Scanning electron microscopy (SEM) and Fourier transform infrared spectroscopy (FT-IR) analysis also supported the same[5].

Mobin *et al.*, investigated a biopolymer namely arabinogalactan (AG) on the protection of carbon steel in 1M HCl medium adopting electrochemical and non-electrochemical methods. Increased inhibition efficiency on increasing the concentration and temperature was noticed. Thermodynamic and activation parameters were calculated followed by surface

analysis by UV–visible spectroscopy, scanning electron microscopy and atomic force microscopy. The experimental results were correlated with quantum chemical and Monte Carlo simulation studies[6].

Xanthan gum (XG) and xanthan gum-graft-poly(acrylamide) (XG-g-PAM) were investigated for its anti corrosive potential for mild steel in 15% HCl by **Biswas *et al.,***. Methods adopted indicated mixed type of inhibition. The adsorption of inhibitor on the metal surface was confirmed by scanning electron microscopy (SEM) and the relationship between structure and its corrosion protection ability was studied by density functional theory (DFT)[7].

The extent of mild steel protection favoured by starch (polysaccharide) was documented by **Mobin *et al.,*** using weight loss and potentiodynamic polarisation techniques in the temperature ranging from 30°C to 60°C. Moderate inhibition efficiency of 66.21% observed for 200 ppm concentration of starch made to study the influence of sodium dodecyl sulfate (SDS) and cetyl trimethyl ammonium bromide (CTAB) in combination with starch which resulted in a synergistic effect favouring physisorption mechanism. The results obtained from both the methods were consistent with each other[8].

Tiu *et al.,* provided an overview on polymeric corrosion inhibitors in oil and gas industries that has the capability of forming metal complexes or undergoing chelation on corrosive reagents resulting in improved corrosion inhibition[9].

Liu *et al.,* synthesised a novel eco-friendly inhibitor, acrylic acid-allylpoly ethoxy carboxylate copolymer (AL15) and tested its inhibition performance on mild steel in sea water medium by means of impedance and polarisation techniques. Increased inhibition efficiency was observed on increasing the concentration. The anti-scaling nature rendered by AL15 on the metal surface was examined by X-ray diffraction (XRD) and scanning electron microscopy (SEM)[10]..

Though the poly methyl aniline (PMA) has been reported as efficient corrosion inhibitor for mild steel, its insolubility has made **Karthikaiselvi *et al.,*** to convert PMA into a water soluble composite poly(vinylpyrrolidone-methyl aniline) using polyvinylpyrrolidine. Later mild steel dissolution in 1M HCl was studied in the presence of synthesised composite by means of weight loss, impedance and polarisation methods. The formation of a surface barrier was confirmed by SEM and EDS analysis[11].

Abdul Rahiman *et al.,* synthesised poly(vinyl alcohol-cysteine) [PVAC], a water soluble composite and investigated its corrosion inhibition efficiency for mild steel in molar

HCl using electrochemical and non-electrochemical methods. Studies made on the effect of time, temperature and concentration resulted with a highest inhibition efficiency of 94% at a concentration of 0.6% wt. Best fit was observed from El-Awady adsorption isotherm. Potentiodynamic polarisation study revealed mixed type of inhibition[12].

Zhang *et al.,* prepared different forms of polyaniline (PANI) comprising of hydrofluoric acid and camphorsulfonic acid and added to epoxy coatings. Evaluation of corrosion inhibition studies concluded that the camphorsulfonic acid-doped PANI coating possess best performance compared to other systems under investigation. The protective layer imparted by PANI coatings was supported by scanning electron microscopy (SEM) and X-ray photoelectron spectroscopy (XPS)[13].

Biswas *et al.,* grafted Gum Acacia (GA) with polyacrylamide to investigate its corrosion inhibition efficiency for mild steel in 15% HCl. Maximum inhibition efficiency of 94.08% was obtained for an optimised combination of 1g acacia and 3g acrylamide at 0.3 g/L. Langmuir adsorption isotherm was found to be the best fitted isotherm. Mixed mode of inhibition was revealed from polarisation data. Morphological examination made by field emission scanning electron microscopy (FE-SEM), energy dispersive x-ray spectroscopy (EDX) and atomic force microscopy (AFM) also conveyed the same[14].

Biopolymers namely Iota-carrageenan (IC) and inulin (INU) were tested for its inhibition on mild steel in 0.5 M H_2SO_4 by **Nirmala Devi *et al.,***. Parallel relationship between concentration and inhibition efficiency was found. Evaluation of thermodynamic parameters and activation parameters gave mechanistic information. Comparison of uninhibited and inhibited specimens were done based on atomic force microscopy (AFM), scanning electron microscope (SEM) and energy dispersive X-ray spectroscopic (EDX)[15].

A non-toxic, low cost biopolymer, chitosan was investigated as corrosion inhibitor for mild steel in 1 M sulfamic acid by **Gupta *et al.,***. An efficiency of 73.8% was observed for 200 ppm concentration of chitosan, whereas a combination with 5 ppm KI gave a pronounced inhibition efficiency of 90% experiencing a synergistic effect. Increased charge transfer resistance and decreased cathodic and anodic reactions were revealed from electrochemical measurements. Surface studies were supported by atomic force microscopy (AFM) and scanning electron microscopy (SEM)[16].

Less expensive coating on carbon steel surface by polypyrrole (PPy) layers was done by **El Jaouhari *et al.,*** adopting electro synthesis method. The morphology of the deposited film was studied using Raman spectroscopy, scanning electron microscopy (SEM) and X-ray

photoelectron spectroscopy (XPS) followed by its corrosion resistance with the aid of open circuit potential (OCP), electrochemical impedance spectroscopy (EIS) and atomic absorption spectroscopy[17].

El-Deeb *et al.,* reporting a mixed type of inhibiton from potentiodynamic polarisation measurements while experimenting the inhibition effect of monomer 3-(12-sodiumsulfonate dodecyloxy) and its polymer analog poly 3-(dodecyloxy sulfonic acid) aniline on aluminium coupons in 0.5 M HCl. Best fit with Langmuir and Frumkin adsorption isotherms were obtained followed by the determination of thermodynamic parameters for adsorption and dissolution process[18].

The corrosion inhibition efficiency of sodium alginate (SA), a biopolymer was reported by **Obot *et al.,*** for API X60 steel under neutral 3.5% NaCl medium adopting gravimetric and electrochemical techniques. Increased inhibition efficiency with concentration was observed. Contact angle measurements projected reduced corrosion kinetics. Interaction of SA with steel surface was confirmed by SEM-EDS followed by UV–vis and ATR–IR measurements confirming the interaction through carboxylate oxygen. Further atomic level insights were studied by quantum chemical calculations and Monte Carlo simulations[19].

Mobin *et al.,* utilised polysaccharide obtained from Plantago ovata for carbon steel protection in 1M HCl. Gravimetric, potentiodynamic polarization, electrochemical impedance spectroscopy (EIS), scanning electron microscopy (SEM), atomic force microscopy (AFM), UV–vis spectroscopy and FTIR were adopted to study the corrosion inhibition phenomena. Spontaneous adsorption was revealed from thermodynamic and activation parameters followed by mixed type of inhibition from polarisation technique[20].

Nirmala Devi *et al.,* synthesised a novel polyamidoaminoepichlorohydrin resin to evaluate its corrosion inhibition performance on mild steel by mass loss method, impedance and polarisation techniques. The adsorption of resin followed Langmuir adsorption isotherm. SEM, AFM, FT-IR and XRD were adopted to study the surface changes[21].

Zhu *et al.,* reported a simple and facile method to prepare poly(aniline-co-5-aminosalicylic acid) (PAASA) nanofibers which was characterised by FT-IR, UV-Vis, XPS, SEM and TEM. It is a promising material with significant electrochemical corrosion protection in neutral environment[22].

Sounthari *et al.,* synthesised polyester–groundnut shell composite (PEGNS) by means of ultrasonication method to evaluate its corrosion reduction nature in 1 M H_2SO_4 for mild steel. Inhibition efficiency showed a direct relationship with concentration and inverse with the temperature. Formation of a protective film was suggested from electrochemical parameters

like R_t, C_{dl}, I_{corr}, E_{corr}, b_a and b_c. The experimental results were best fitted with Langmuir adsorption isotherm[23].

From the survey of literature it is evident that much work has not been carried out with water soluble polyesters as corrosion mitigators for mild steel in acid media. Before stepping into the discussion, it is precise to mention about bio-based raw materials which has gained a detailed insight in synthesising polymers. Several bio-based polymers like polyesters[24,25] polyamides[26], polyurethanes has been reported in various aspects so far. In specific, biocompatible and biodegradable nature of polyesters has made it to deserve its position in biomedical and tissue engineering fields[27,28]. Such polyesters from glycerol and dicarboxylic acids like sebaccic acid[29,30], succinic acid[31], adipic acid[32] has been remarkably known for its applications. In continuation, the present work has been targeted towards the novel polyesters whose biodegradability in specific, will promise for a successful future and projects itself as an excellent material for emerging trends[33]. Besides its fleeting applications, as a challenge and desire to find an ultimate polymer as a replacement for existing toxic inhibitors, the present work has been framed to investigate the anticorrosive behaviour of linear aliphatic water soluble polyesters (synthesis described in chapter II) in 0.5 M H_2SO_4.

3.2 EXPERIMENTAL METHODS

3.2.1 Inhibitors

A series of aliphatic polyesters were synthesised by polymerising dicarboxylic acids with triol (synthesis described in chapter-II) and used as inhibitors for the present study whose polymeric skeleton can be represented as,

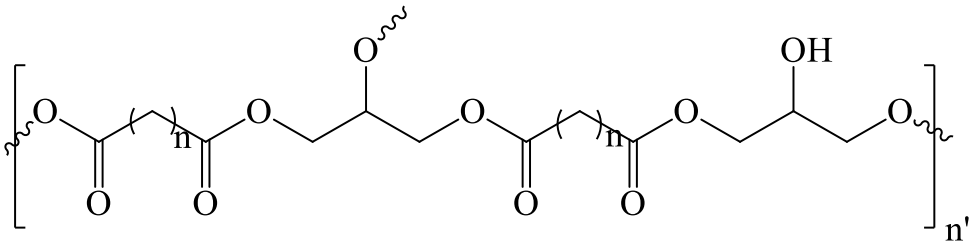

Where **n=1**, Poly (glycerol malonate) **(PGM)**

n=2, Poly (glycerol succinate) **(PGS)**

n=3, Poly (glycerol glutarate) **(PGG)**

n=4, Poly (glycerol adipate) **(PGA)**

n=5, Poly (glycerol pimelate) **(PGP)**

n=6, Poly (glycerol suberate) **(PGSU)**

n=7, Poly (glycerol azelate) **(PGAZ)**

n=8, Poly (glycerol sebaccate) **(PGSE)**

3.2.2 Material preparation

A flat mild steel sheet was mechanically compressed into coupons of 1 cm x 3 cm x 0.08 cm dimension for non-electrochemical techniques and a cylindrical rod embedded with Teflon with an exposed area of 0.785cm^2 was employed for electrochemical techniques. The specimens were tested and its chemical composition was found to be C (0.084%), Mn (0.369%), Si (0.129%), P (0.025 %) , S (0.027%) , Cr (0.022%) , Mo (0.011%), Ni (0.013%) and Fe (99.32%).

The specimens were abraded with different grades of silicon carbide sheets, degreased with acetone, washed with water, dried and stored in moisture free desiccator prior to use.

3.2.3 Corrodent solution

Analar grade sulphuric acid was used for the preparation of 0.5 M H_2SO_4 which was consumed in a proportion of 100 ml as a test solution for all consecutive studies.

3.2.4 Corrosion monitoring techniques

(i) Gravimetric measurements

Gravimetric measurements were performed using 100 ml of 0.5 M H_2SO_4 as a test solution in stagnant aerated condition at $\pm$ 30^o C. The precleaned and weighed mild steel coupons were suspended in triplicates with the help of glass hooks. Care was taken to ensure the complete immersion. After three hours of duration the immersed specimens were removed, washed with distilled water, dried and weighed. The weight loss was taken as the difference in the weight of mild steel before and after exposure to different test solutions with the help of semi micro analytical balance with a precise accuracy.

To study the effect of temperature similar tests were carried out in a thermostatic water bath maintained at a temperature range of 303 K-333 K for a duration of 1 hour. The corrosion parameters such as inhibition efficiency (%), corrosion rate (CR), surface coverage (Θ) and thermodynamic parameters were calculated according to the following formulas.

(a) Efficiency of inhibitor

From the initial and final weight of the specimens, weight loss with and without inhibitors were calculated. From this, the efficiency of the inhibitor was calculated using the formula,

$$\text{Inhibition efficiency}(\%) = \frac{\text{weight loss without inhibitor} - \text{weight loss with inhibitor}}{\text{weight loss without inhibitor}} \times 100 \qquad (1)$$

(b) Corrosion rate

The average corrosion rate was determined by considering the initial total surface area of the specimen and the mass lost during the test period using the following equation,

$$\text{Corrosion rate}\,(\text{gcm}^{-2}\text{hr}^{-1}) = \frac{534 \times \text{weight loss (gms)}}{\text{Density x Area (cm}^2\text{) x Time (hrs)}} \times 100 \qquad (2)$$

The surface coverage (θ) has been calculated using the formula

$$\text{Surface coverage } (\theta) = \frac{\text{Inhibition effeciency } (\%)}{100} \qquad (3)$$

(c) Activation energy (E_a)

The activation energy was calculated graphically by plotting log (corrosion rate) Vs 1000/T (K) for a temperature range of 303 K - 333 K in 0.5 M H_2SO_4 medium with and without inhibitors at selected concentrations. From the slope of the straight line E_a was determined using the following expression,

$$Ea = 2.303 \times 8.314 \times \text{slope} \qquad (4)$$

(d) Free energy of adsorption

The below representation was used to determine the free energy of adsorption ΔG^o_{ads} from the equilibrium constant,

$$K = \frac{1}{55.5} \exp(-\Delta G^o / RT)$$

where,

$$K = \frac{\theta}{1-\theta} \text{ (From Langmuir)}$$

$$\Delta G^o_{ads} = -RT \ln(55.5K) \qquad (5)$$

(ii) Electrochemical techniques

Polarisation and electrochemical impedance spectroscopic studies were carried out in a conventional three electrode cell assembly comprising of mild steel rod with an exposed area of 0.785 cm^2 as working electrode, a platinum and saturated calomel electrode as counter and reference electrode with an aid of ivium compactstat potentiostat installed with ivium software.

(a) Electrochemical impedance spectroscopy

Electrochemical impedance spectroscopy (EIS) is the most important routine technique applied to evaluate the corrosion mechanism and fundamental parameters of electrochemical reactions.

The EIS measurements were performed at constant potential in a frequency range of 10 KHZ to 0.01 HZ with an amplitude of 10 mV as excitation signal with a test solution of 0.5 M H_2SO_4. The real part (Z') and the imaginary part ($Z^{''}$) were measured at various frequencies. A plot of $Z^{'}$ vs $Z^{''}$ were made. From the plot, the charge transfer resistance (Rct) and double layer capacitance (Cdl) were calculated .The percentage inhibition efficiency were calculated from charge transfer resistance values by the following expression[34],

$$\text{Inhibition efficiency}(\%) = \frac{R_{ct(inh)} - R_{ct(Blank)}}{R_{ct(inh)}} \times 100 \quad (6)$$

where $R_{ct(inh)}$ and $R_{ct(blank)}$ is the charge transfer resistance in the presence and absence of inhibitor

(b) Potentiodynamic polarization technique

Electrochemical polarisation studies for mild steel rod in 0.5 M H_2SO_4 with and without inhibitors were performed by recording anodic and cathodic potentiodynamic polarisation curves. Polarisation plots were obtained in the electrode potential range of -200 to +200 mV at a scan rate of 1mV/sec. The log of current and the corresponding potentials were fed into the plotter and potential E vs log I was plotted. By extrapolating the experimental cathodic and anodic curves to the potential axis, corrosion current density (I_{corr}) was deduced from which the inhibition efficiency can be calculated by using the below relation[35],

$$\text{Inhibition efficiency}(\%) = \frac{I_{corr(blank)} - I_{corr(inh)}}{I_{corr(blank)}} \times 100 \quad (7)$$

where $I_{corr(blank)}$ and $I_{corr(inh)}$ indicates the corrosion current densities in uninhibited and inhibited medium.

3.2.5 Morphological analysis

(i) FT-IR spectra of corroded plates

Detailed insight on adsorption of inhibitors on the metal surface was made by exposing the working specimens immersed in the corrodent containing optimum concentration of selected additives such as PGG and PGP to the FTIR analysis with an aid of FT-IR spectrometer (Schimadzu – IR Affinity 1).

(ii) X-ray diffraction analysis

The mild steel coupons of the present investigation was immersed in 0.5 M H_2SO_4 medium in the absence and presence of 1000 ppm concentration of PGG and PGP polyesters for 3 hours and the adsorption of inhibitors on the specimens were analysed by recording X-ray diffraction measurements in the angle range of $10^o < 2\Theta < 80^o$ using Brucker X- ray diffractometer.

(iii) Scanning electron microscopy (SEM) & Energy dispersive X-ray spectroscopy (EDS)

As a supporting evidence the coverage of mild steel surface in uninhibited and inhibited test solution (PGG, PGP) at an optimised concentration of 1000 ppm were examined by Zeiss SEM analytical instrument. In addition EDS were recorded for the similar samples in order to execute the % chemical composition of the elements.

(iv) Atomic force microscopy

Atomic force microscopy is an important surface analytical technique that projects the roughness values of the mild steel specimens. As an initiative the specimens immersed in the corrodent with PGG and PGP as well as without inhibitors for 3 hours were elicited, washed, dried and analysed using multimode scanning probe microscope (NT-MDT).

(v) X-ray photoelectron spectroscopy (XPS)

The elements adsorbed on the metal surface was additionally evidenced from X-ray photoelectron spectroscopy (XPS) by using the mild steel specimens of appropriate dimensions, which after proper pretreatment was allowed to suspend in uninhibited and PGP inhibited test medium for a duration of three hours, retrieved and taken for analysis. The samples were tested with an aid of Model no-Axis ultracompany – Kratos Analytical country-UK, with a source of Al K alpha (1486 eV). The datas obtained were quantified using casaxps software.

3.3 RESULTS AND DISCUSSION

3.3.1 Corrosion monitoring techniques

3.3.1.1 Gravimetric measurements

It is a preliminary basement technique used to evaluate the corrosion inhibition of mild steel specimens of appropriate dimensions in 0.5 M H_2SO_4 medium varying the concentrations in the intervals of 10, 50, 100, 500, 1000, 1500 ppm. Since decreased inhibition efficiency was observed at 1500 ppm, 1000 ppm concentration was optimised. From the data represented in the **Table 3.1**, it is clear that the introduction of polyesters at various concentrations caused a significant reduction in the corrosion of mild steel which might be due to the sufficient adsorption and wider coverage of inhibitor molecules[36] thereby blocking the active sites of acid attack[34]. Maximum inhibition efficiency was obtained for PGSE around 77.63 % as displayed in **Fig. 3.1**. Though the polymers are expected to behave as efficient inhibitors, the absence of aromatic anchoring sites, large molecular size, more number of heteroatoms and bulky structure[37] might cause comparatively less efficiency than remarkable increase. However increase in the length of alkyl chain might bring + inductive (+I) effect to increase electron density thereby facilitating adsorption in the order of PGSE > PGAZ > PGSU > PGP > PGA > PGG > PGS > PGM.

(a) Effect of temperature

Temperature plays an important role in understanding the inhibitive mechanism of the corrosion process. To assess the temperature effect, experiments were performed in the range of 303 K-333 K in uninhibited and inhibited solutions containing selected concentrations of the inhibitor (10, 100, 1000 ppm) for an hour immersed in 0.5 M H_2SO_4. From the results depicted in **Table 3.2**, it is evident that the corrosion rate is a temperature dependent parameter which decreases the inhibition efficiency on increasing the temperature leading to the desorption of inhibitor molecules from the metal surface thereby forcing large surface area of metal to get in contact with acid. This results in the modification of electrostatic interaction occurring between inhibitor molecules and iron interface[38] resulting in enhanced corrosion rate. In general acidic medium is accompanied by the evolution of hydrogen gas with the increase in temperature[29] indicating desorption process.

(b) Thermodynamic and kinetic considerations

Based on the temperature studies, the corrosion rate evaluated was applied in the below mentioned Arrhenius equation to calculate the activation energy E_a, followed by calculating the various activation parameters.

$$\text{Corrosion rate (CR)} = A \exp[(-E_a)/RT \quad (8)$$

where E_a is the activation energy, R is the universal gas constant, K is the pre-exponential constant and T is the absolute temperature. A plot between log corrosion rate vs 1000/T gives Arrhenius plot as shown in **Fig. 3.2** whose slope equal to $-E_a/RT$ enables the calculation of activation energy E_a as given in **Table 3.3**.

From **Table 3.3**, it is predicted that the activation energy E_a in the presence of inhibitors were higher than those in free acid solution indicating lower inhibition efficiencies at elevated temperatures. E_a values range from 51.81 KJ/mol to 61.10 KJ/mol which is lower than the threshold value of 80 KJ/mol required for chemical adsorption. This favours spontaneous adsorption of inhibitor on the mild steel surface attributing to physical adsorption[40]. Moreover the presence of inhibitor induces an energy barrier which opposes the corrosion process and successively reduces the dissolution of mild steel[41].

In order to elucidate the enthalpy of activation ΔH^o and entropy of activation ΔS^o, an alternate form of Arrhenius equation was used in the form of Transition State equation formulated as,

$$\text{Corrosion rate (CR)} = \frac{RT}{Nh} \exp(\Delta S^o / R) \exp(-\Delta H^o / RT) \quad (9)$$

where h, N, R, ΔH°, ΔS°, indicates Planck constant, Avogadro number, universal gas constant, enthalpy of activation and entropy of activation. A plot of log (corrosion rate/T) vs 1/T as shown in **Fig. 3.3** for various inhibitors gave a linear relationship with a slope of $(-\Delta H^\circ/2.303R)$ and an intercept of $(\log(R/Nh) + (\Delta S^\circ/2.303R)$ from which the values of ΔH° and ΔS° were computed and listed in **Table 3.3**.

Inspection of these data shows the shift towards large and negative values of entropy ΔS°, revealing that the activated complex in the rate determining step represents an association rather than dissociation meaning that decrease in disorder takes place on going from reactants to activated complex as reported by **Fouda *et al.*,**[42]. The positive values of ΔH° reflects the endothermic nature of mild steel dissolution thereby providing better coverage area for inhibitor surface and minimising the dissolution phenomena[43].

The change in free energy of activation (ΔG^{o}_{ads}) can be deduced for each temperature by applying the below equation,

$$\Delta G^{o}_{ads} = \Delta H^{o}_{ads} - T\Delta S^{o}_{ads} \quad (10)$$

where ΔH°_{ads} and ΔS°_{ads} are the enthalpy and entropy changes of adsorption process, respectively. The calculated values of ΔG^{o}_{ads} displayed in **Table 3.3** shows minimum increase with increase in temperature indicating that the activated complex is unstable and the probability of its formation decreased somewhat with increase in temperature leading to lesser efficiency[39].

(c) Adsorption isotherms

The mode of adsorption of the inhibitors on the mild steel surface can be dealt in detail by fitting the experimental data obtained from the gravimetric measurements into various adsorption isotherms as summarised below from which adsorption isotherm parameters can be elicited.

Adsorption isotherm	Representation	Verification plot
Langmuir	$\frac{C}{\theta} = \frac{1}{K_{ads}} + C$	$\frac{C}{\theta}$ vs C
Temkin	$\log K + \log C = \frac{-2a\theta}{2.303}$	Θ vs log C
El-Awady kinetic model	$\log(\Theta/1-\Theta) = \log K + y\log C$	$\log(\Theta/1-\Theta)$ vs log C
Flory-Huggins	$\log(\Theta/C) = \log K + x\log(1-\Theta)$	$\log(\Theta/C)$ vs $\log(1-\Theta)$

The values of regression coefficient R^2 confirmed the validity of this approach.

(i) Langmuir adsorption isotherm

It is a linear relationship between C/Θ vs C as shown in **Fig. 3.4** and the resulting parameters are presented in **Table 3.4**. This model assumes that the solid surface contains a fixed number of adsorption sites and each site holds one adsorbent[44]. The R^2 values close to unity indicate strong adherence and the best fit. Though the linearity and R^2 values may suggest the adsorption, the considerable deviation of the slope from unity indicated that the adsorption of large polymer molecules on the metal surface may interact by mutual repulsion (or) attraction which is against Langmuir postulates where it is stated that adsorbed molecule do

not interact with one another as reported by **Karthikaiselvi *et al.*,**[39]. Moreover the type of adsorption process taking place on the electrode surface can be justified by the values of K_{ads} and ΔG_{ads}^{o}. The higher value of K_{ads} reflects the higher adsorption ability of the inhibitor whereas the negative values ΔG^{o}_{ads} indicates spontaneous and stable adsorption on the mild steel surface to an extent[42]. ΔG^{o}_{ads} calculated ranges from -36.71 KJ/mol to -35.71 KJ/mol suggesting the adsorption of inhibitors as a combined mechanism ie., predominantly physisorption and partly chemisorption as reported by **Ministry *et al.*,**[46,47].

(ii) Temkin adsorption isotherm

The extent of Temkin adsorption isotherm as per the equation shown above is evaluated by plotting Θ vs log C as shown in **Fig. 3.5**. From **Table 3.5** it is evident that the R^2 values close to unity supports monolayer adsorption and the positive values of activation parameter 'a' supports attraction rather than repulsion of adsorbed layer[40].

(iii) El-Awady adsorption isotherm

As shown in **Fig. 3.6**, a plot of log C vs log $\frac{\theta}{1-\theta}$ and the parameters listed in the **Table 3.6** evaluates the validity of this approach. If the reverse of slope 1/y is less than unity it implies the multilayer formation and 1/y greater than unity suggests that the inhibitor occupies more than one active site[48]. The data displayed in **Table 3.6** reveals that 1/y is greater than unity which enables the inhibitor to occupy more than one active site.

(iv) Flory - Huggins adsorption isotherm

Flory-Huggins adsorption isotherm can be formulated as mentioned above where x=1/a, the size parameter which is a measure of the number of adsorbed water molecules substituted by an inhibitor molecule. From **Table 3.7**, it is interpreted that the positive values of size parameter x displaces more than one water molecule from the mild steel surface due to the bulky adsorbed species[40]. The plot of log (1-Θ) vs log (Θ/C) as shown in **Fig. 3.7** shows a non-linear relationship which strictly regrets Flory-Huggins isotherm.

The perfect fit of the adsorption data with various adsorption isotherms can be decided mainly based on R^2 value which confirms the validity of this approach rather than other parameters. The best fit was observed with Langmuir[49] isotherm based on the linear plots and with R^2 values close to unity.

(d) Thermodynamic parameters

Most of the methods can enable us to get information regarding the interaction of studied inhibitor and the metal surface at different temperatures. But the suggested method is the usage of thermodynamic model with various thermodynamic parameters such as ΔH^o_{ads}, ΔS^o_{ads} and ΔG^o_{ads}.

ΔH^o_{ads} and ΔS^o_{ads} are the important parameters calculated from van't Hoff equation represented as,

$$\ln (K)_{ads} = - \Delta H^o_{ads} / RT + \Delta S^o_{ads} / T + \ln \frac{1}{55.5} \quad (11)$$

As shown in the **Fig. 3.8**, a plot of log K_{ads} vs $\frac{1}{T}$ gave a straight line with slope equal to (ΔH^o_{ads} / 2.303R) and an intercept of (ΔS^o_{ads} / 2.303R) + log $\frac{1}{55.5}$ from which ΔH^o_{ads} and ΔS^o_{ads} were calculated and presented in the **Table 3.8**.

Gibbs Helmholtz equation also enables the determination of enthalpy of adsorption ΔH^o_{ads} according to the following relationship

$$\Delta G^o_{ads} / T = \Delta H^o_{ads} / T + A \quad (12)$$

A straight line observed in the plot of ΔG^o_{ads} / T vs 1/T shown in the **Fig. 3.9**, enables the calculation of standard enthalpy of adsorption (ΔH^o_{ads}) which is simply equal to the slope. The values displayed in the **Table 3.8** are in good agreement with each other.

Another approach to deduce ΔH^o_{ads} and ΔS^o_{ads} is from basic thermodynamic equation represented as

$$\Delta G^o_{ads} = \Delta H^o_{ads} - T\Delta S^o_{ads} \quad (13)$$

A linear straight line was obtained from the plot of ΔG^o_{ads} vs T with a slope equal to $-\Delta S^o_{ads}$ and an intercept of ΔH^o_{ads} as displayed in **Fig. 3.10**.

With the help of data summarised in **Table 3.8**, it is generally analysed that the complex process is most favoured by thermodynamic parameters ie., ΔH^o_{ads} and ΔS^o_{ads}. The negative sign of ΔH^o_{ads} enables exothermic adsorption nature which is an evidence for lower protection efficiency when temperature increases[50]. By considering the values of ΔH^o_{ads} physisorption can be distinguished from chemisorption where the ΔH^o_{ads} values for the former case is lower than -40 KJ/mol whereas the latter reaches 100 KJ/mol. Investigating the data represented, ΔH^o_{ads}

ranging from -22.51 KJ/mol to -7.13 KJ/mol supported physisorption and the positive values of ΔS^{o}_{ads} endeavoured the adsorption of inhibitor molecules as reported by **Rubaye *et al.*,**[51].

General observation reveals that ΔG°_{ads} upto -20 kJ/mol represents the physisorption (electrostatic interaction between charged molecule-charged metal) whereas ΔG°_{ads} above -40 kJ/mol indicates chemisorption (charge transfer or sharing from inhibitor molecule to metal). The present investigated values of ΔG°_{ads} between -28.51 KJ/mol to -30.61 KJ/mol elucidated that the adsorption process of the evaluated inhibitors in 0.5 M H_2SO_4 medium on the mild steel surface may involve complex interactions but predominantly physisorption[50].

3.3.1.2 Electrochemical techniques

(i) Electrochemical impedance spectroscopy

(a) Nyquist plot

Impedance method provides information about the kinetics of the electrode processes and simultaneously about the surface properties of the investigated systems. EIS spectra of mild steel in uninhibited and inhibited with selected concentrations of the inhibitor in 0.5 M H_2SO_4 are shown in **Figs. 3.11-3.18**. The equivalent circuit model used to fit the experimental data was Randle's model as shown in **Fig. 1**

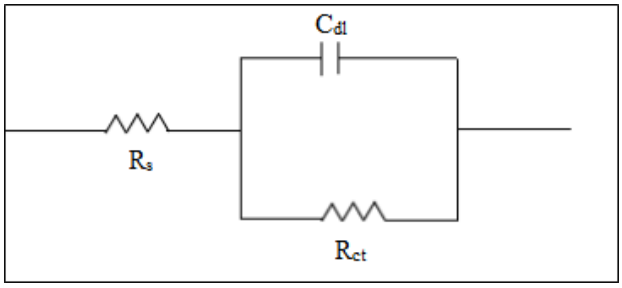

Fig. 1 Equivalent circuit used to simulate the data

where solution resistance, charge transfer resistance and double layer capacitance are represented as R_s, R_{ct} and C_{dl}.

The Nyquist plots shown are characterised by one single capacitive loop which are deviated from perfect semicircle shape due to the frequency dispersion and attributed towards roughness and non-homogeneity of electrode surface which is a characteristic phenomena of solid electrodes[45] leading to dispersion effect[52].

It is evident from **Table 3.9**, the impedance response for the mild steel increased with increase in concentration of the inhibitors. The addition of polyesters to the corrosive medium increased the charge transfer resistance (R_{ct}) which in turn decreased the double layer capacitance (C_{dl}). The value of charge transfer resistance (R_{ct}) obtained is a measure of electron transfer across the metal-solution interface and inversely proportional to the corrosion rate suggesting strong resistance against corrosion. The resulting capacitive loop intersects the real axis at higher and lower frequencies. At high frequency the intercept corresponds to solution resistance (R_s), at low frequency it corresponds to the sum of $R_s + R_{ct}$. This difference predicts R_{ct}[35].

A decreased C_{dl} results due to the replacement of already adsorbed water molecules (high dielectric constant) on metal surface by added inhibitors (low dielectric constant). It is reported[49] that the capacitance is inversely proportional to the thickness of the double layer which strictly suggests that the inhibitor molecules are adsorbed on the metal-solution interface. Such C_{dl} values can be computed by the following relation

$$C_{dl} = 1/2\pi f_{max} R_t \qquad (14)$$

where f_{max} is the frequency at which imaginary component is maximum.

On increasing the concentration from 10 ppm to 1000 ppm, there was a gradual increase in the diameter of the semicircles reflecting increased R_{ct} values from 15.8 ohm cm^2 to 48.5 ohm cm^2 and increased inhibition efficiency which was attributed to the formation of protective layer on the mild steel surface[53].It was obviously noted that the corrosion process involved two steps in any of the electrochemical processes at the electrochemical interface. First reaction involves oxidation of the metal (charge transfer process) and second the diffusion of metallic ions from the metal surface to the solution thereby producing a barrier for the metal to diffuse out and this barrier increases with concentration resulting in enhanced inhibition efficiency[54]. It is clear that when the immersion time increased, R_{ct} value increased with decrease in C_{dl}. But when the immersion time is further enhanced it experiences a sudden decrease in R_{ct} value and increase in C_{dl} due to the instability or desorption of adsorbed layer[41]. This confirms that the data were recorded in appropriate duration.

(b) Bode plot

The electrochemical behaviour of the mild steel specimens immersed in acid medium can be relevantly understood with the aid of bode plots. It is a general representation that the

bode plots represent the number of peaks pertaining to the number of time constants. If a bode plot is accompanied with one peak then the system has one time constant with parallel relationship between number of peaks and time constants. Bode plots obtained from EIS analysis of mild steel immersed in 0.5 M H_2SO_4 containing selected concentrations of the polymers are shown in **Figs. 3.19-3.26** in which the single peaks obtained indicates that the EIS data were fitted in one time constant model. Moreover the only one phase maximum obtained indicates only one relaxation process[55] which would be the charge transfer process taking place at the metal electrolyte interface which means that the corrosion rate is reduced in presence of inhibitors.

The experimental data obtained for Nyquist plot were utilised to plot bode plots where an increased phase angle shift was consecutively noticed with increase in concentration of the inhibitors. The maximum phase angle for a metal solution corrosion system represented by simple RC parallel combination should be -90^o for an ideal capacitor. From the plots it is concluded that the phase angle ranging up to -60^o shows slight deviation from capacitive behaviour suggesting the inhibitive performance of the added polymer to an extent. However the change in phase shift suggests the formation of surface barrier thereby changing the electrode interfacial structure and minimising the corrosion.

(ii) Potentiodynamic polarisation studies

From the Tafel curves shown in **Figs. 3.27-3.34**, changes corresponding to corrosion current density (I_{corr}) , corrosion potential (E_{corr}), anodic Tafel slope (b_a), cathodic Tafel slope (b_c) were deducted and listed in the **Table 3.10**.

From the data it is evident that inhibition efficiency increases with increase in concentration favouring adsorption. In general, acidic medium is associated with the anodic corrosion reaction with the passage of metal ions into the solution and cathodic corrosion reaction by means of hydrogen evolution or reduction of oxygen. The added inhibitor can affect cathodic (or) anodic reaction (or) both. In the present investigation the added inhibitor did not reveal any predominant shift in E_{corr} value insisting that the added inhibitors were of mixed type. Displacement of E_{corr} value > 85 mV with reference to blank, makes the inhibitor to behave as either cathodic or anodic whereas E_{corr} less than $\pm$ 85 mV enables mixed type inhibitors[49]. The maximum displacement observed in this study was 67.3 mV revealing the mixed nature of the inhibitors.

The lower values of corrosion current densities facilitates slow electron transfer thereby reducing the corrosion rate[41]. **Figs. 3.27-3.34** shows the effect of added polyesters on the cathodic and anodic polarisation curves resulting in reduced anodic dissolution and retarded hydrogen evolution. In addition the cathodic and anodic Tafel slopes exhibited slight changes indicating the influence on both the reactions but predominantly cathodic reactions.

Adsorption is generally an accepted mechanism in corrosion inhibition studies. The adsorption of inhibitor can alter the rate of corrosion in two different ways,

(i) by decreasing the available reaction area known as geometric blocking effect

(ii) by modifying the activation energies of cathodic and (or) anodic reactions that occur in uninhibited metal by adding inhibitors.

However it is tedious to discriminate between inhibiting effect related to geometric blocking and energy effects. Theoretically it is predicted that geometric blocking effect is stronger than the energy effect when there is no predominant shift in E_{corr} value after the addition of inhibitors. Based on this it was concluded that the possible mechanism undergone was geometric blocking effect. The results obtained by the electrochemical and non-electrochemical techniques were in good agreement with each other. Though the slight variation observed in the inhibition efficiency might be due to the occlusion of the metal surface from inhibitor formulation[56].

3.3.1.3 Morphological evaluation

(i) FTIR spectra of surface film

The extent of adsorption and interaction on the mild steel surface by the inhibitor can be certainly assessed by analysing the surface film as shown in **Figs. 3.35 and 3.36**. The observation of FT-IR analysis of mild steel specimens immersed in optimum concentration of the additive PGG manifested a shift of ether linkages from 1147.01 cm^{-1} to 1211.35 cm^{-1} followed by the carbonyl shift from 1710.73 cm^{-1} to 1700.35 cm^{-1} owing the involvement of –C-O-C- stretching and >C=O stretching linkages in adsorption on the metal specimen. PGP was accompanied with a shift of ester group from 1708.13 cm^{-1} to 1731.93 cm^{-1} and ether group from 1178.19 cm^{-1} to 1212.71 cm^{-1}. Both the inhibitors exhibited modified bands at 3325.05 cm^{-1} (PGG inhibited) and 3215.88 cm^{-1} (PGP inhibited) corresponding to shift in –OH stretching implying the involvement of hydroxyl moieties in surface coverage. All these

prominent shifts confirmed the involvement of functional groups in adsorption on the metal surface.

(ii) X-ray diffraction pattern (XRD)

The X-ray diffraction studies is a method used to assess the adsorption of inhibitor on the metal specimens. Carbon steel specimen immersed in aggressive acid medium has experienced peaks corresponding to magnetite (Fe_3O_4), FeOOH (goethite), Fe_2O_3 (hematite) and Fe (iron) matrix in the report stated by **Abboud *et al.,*** [57]. The XRD patterns shown in the **Fig. 3.37** pertains to the mild steel specimens immersed in 0.5 M H_2SO_4, PGG and PGP inhibited medium. All the patterns experienced peaks approximately at 44^o and 82^o owing to the presence of FeOOH and Fe matrix. But the comparison of blank XRD pattern with inhibited ones, clearly showed the decreased intensity of the above mentioned peaks in case of PGG and PGP which is a supporting evidence that the added inhibitor has formed a surface layer on the mild steel surface which could be still evidenced from the forth coming morphological studies.

(iii) Scanning electron microscopy (SEM) & Energy dispersive X-ray spectroscopy (EDS)

The inhibition efficiency results from the mass loss method and electrochemical techniques due to the formation of a film barrier on the metal surface is elicited by the SEM analysis as revealed in the **Fig. 3.38(a-c)**. On examining the specimens immersed in 0.5 M H_2SO_4 (**Fig. 3.38(a)**) severe metal dissolution has been observed which is evident from its cavities, roughness and inhomogeneous surface[58]. On addition of 1000 ppm of respective polymers in corrosive medium, corrosion rate was significantly decreased which was due to the interaction of polymeric grains[59] on the metal surface occupying the cavities thereby leading to a relative smooth homogeneous surface paving way for reduced corrosion rate as clearly depicted in **Fig. 3.38 (b,c)**. From the SEM images, it can be concluded that the surface of PGP inculcated with a better smoothy appearance than PGG is expected to exhibit higher inhibition efficiency which is in agreement with other measurements.

Based on the elemental composition listed in the **Table 3.11**, a valuable information about the surface coverage can be retrieved. From the image shown in **Fig. 3.38(a)** it can be seen that the working specimen has undergone disturbance in aggressive medium[60]. The higher weight % of oxygen (31.58) and iron (64.87), obtained for the specimens immersed in 0.5 M H_2SO_4 confirmed the formation of iron oxide, the corrosive product thereby increasing the iron dissolution. On the other hand the images represented in **Fig. 3.38(b,c)**, reveals the fact that the added polymers has been adsorbed on the mild steel surface in turn retarding the

dissolution of iron and hindering the formation of corrosive product which is additionally evident from the carbon signals.

(iv) Atomic force microscopy (AFM)

The surface morphological evaluation of mild steel specimens are additionally credited by the mean square value projected from AFM analysis. **Fig. 3.39(a-c)** illustrate the micrographs in which uninhibited medium acquired roughness value of 224.66 nm implying severe acid attack on the metal surface leading to surface inhomogeneity with facile dissolution[61]. Surface protection exhibited in the form of increased inhibition efficiency from the techniques involved were supported by the decrease in mean square value from 224.66 nm to 163.95nm and 96.75 nm suggesting the formation of protective layer. However lower mean square value of PGP emphasises better formation of surface barrier than PGG owing to more smooth and homogeneous surface with good adsorption of inhibitors.

(v) X-ray photoelectron spectroscopy (XPS)

To examine the adsorption of the added polymeric compound onto the metal surface, XPS analysis was carried out. The XPS spectra C 1s, Fe 2p and O 1s obtained are shown in **Fig. 3.40**. Observation of the plots shows complex nature, corresponding to the different species which were assigned based of deconvolution fitting procedure. From the Fe 2p spectra shown in **Fig. 3.40**, one can observe peaks associated with iron and its various forms like oxides and hydroxides. Fe 2p deconvoluted spectra of blank specimen exhibited a peak at 711.8 eV representing ferric compounds which would result due to the oxidation of ferrous species on the metal surface. However in Fe 2p spectra of PGP inhibited medium, peak observed at 711.9 eV and 714.2 eV could be due to Fe^{2+} existing in either Fe_2O_3 or Fe_3O_4 or FeOOH. Peak observed at higher binding energy, ie., 725.6 eV corresponds to the satellite peak indicating the existence of iron in divalent state. This clearly states that instead of getting oxidised from Fe (II) to Fe (III), the added PGP has got the capability of forming Fe(II)-PGP complex on the metal surface which is stable and insoluble. The ghost structure noticed at the higher binding energy side could be due to the subsequent oxidation of mild steel surface. The O 1s spectra recorded for blank specimen revealed two peaks at 529.6 eV and 532.8 eV corresponding to O^{2-} and OH^-. O 1s spectra of PGP inhibited mild steel sample shown in **Fig. 3.40**, can be fitted into a well-defined peak around 532 eV with a decreased intensity compared to blank, which corresponds to the oxygen of adsorbed water molecules or oxygen atom attached to the carbon atom (-C=O, -CO-) or –OH as the contribution made by the oxygen atom from a molecule is

inseparable[62-64]. Thus the oxygen atom would have involved in the formation of film on the metal surface. The C 1s spectra displayed in **Fig. 3.40**, showed two prominent peaks similar in both blank and PGP inhibited mild steel sample. It is quite difficult to differentiate. But the difference in the area of the peak assumes that the first peak at lower binding energy 285.5 eV could be attributed to –C-C-, -C=C-, -C-H- bonds present in the added additive as well as –C-O and –C=O, -OH groups. The second peak at 288 eV ie., large binding energy corresponded to carbonyl form of carbon or C^{+}–O form resulting from the protonation of oxygen atom. Thus the above analysis carried out shows the adsorption of inhibitor on the metal surface endeavouring the formation of protective film.

3.3.1.4 Mechanism of corrosion inhibition

The mechanistic action of inhibitors in acid solution is generally believed to take place on the metal surface either by blocking cathodic or anodic or both the reactions. These polymers inhibit the acid dissolution of mild steel by adsorption at Fe-acid solution interface. In acidic medium, polymers exists as protonated species which could adsorb either on the cathodic or anodic sites of mild steel thereby decreasing the evolution of hydrogen or anodic dissolution of mild steel. The high performance of a polymer is attributed due to its multi functionality, reactive sites, molecular size and many. However a polymer can interact with the metal by the following ways[65]

(i) electrostatic interaction between charged molecules and charged metal

(ii) interactions of π electrons with metal

(iii) Interaction of the unshared pair of electrons of the molecule with metal

(iv) combination of all

The possible mechanism can be postulated based on the fact that iron exposed to the environment results in the formation of oxide layer on the surface which can be destroyed in the presence of dilute sulphuric acid where the iron oxide films interact with the sulphates resulting in a complex $Fe_2(SO_4)_3(H_2O)_{n\ ads}$ which gets desorbed from the metal surface due to its solubility thereby leaving the surface for further attack by SO_4^{2-} ions.

$$4Fe + nH_2O + 3O_2 \longrightarrow 4Fe_2O_3(H_2O)_n$$

$$Fe_2O_3(H_2O)_n + 3HSO_4^- + 3H^+ \longrightarrow Fe_2[(SO_4)_3(H_2O)_n]_{ads}$$

At this stage the added polymer exists in poly cationic form (P^{+}). If the added polymer is neutral, it would undergo donor acceptor interaction between the unshared electron pair of oxygen heteroatom to form a bond with vacant d-orbital of Fe on the mild steel surface leading to the formation of a barrier[66]. If not, the complex present in the acid medium which is

positively charged leads to a repulsion between them. Hence specific adsorption of bisulphate ion interacts electrostatically with the polycation leading to the following complex and enhanced protection.

$$Fe_2[(SO_4)_3(H_2O)_n]_{ads} + HSO_4^- + P^+ \longrightarrow Fe_2H[(SO_4)_4(H_2O)_n\ P^+]_{ads}$$

The hydrophobic interaction of the alkyl groups decrease the available H_2O molecules to interact with other hydrophobic tails. This is the way how aliphatic long chain alkyl moieties can decrease the amount of aggressive ions affecting the metallic surface thereby rendering large surface area and blanketing the entire metal surface. The inhibition of mild steel occurring through the proposed mechanism as shown in **Fig. 3.41**. was supported by the formation of film on the surface characterised by FT-IR, XRD, SEM, EDS and its extent was validated by the roughness values projected by the AFM analysis.

3.3.1.5 Evaluation of the inhibitors

It is a general fact that the inhibition rendered by most of the inhibitors depend on many factors like active adsorption centres, charge density, molecular size, pi-electron density, number of heteroatoms and the electrolyte. In the present discussion, a series of polyesters namely PGM, PGS, PGG, PGA, PGP, PGSU, PGAZ and PGSE were synthesised. As reported by most of the researchers, an organic compound containing functional groups with heteroatoms generally possess the ability of getting anchored on the metal surface. However polymeric materials basically due to its multiple functional sites has the capability of displacing more water molecules from the metal surface favouring good adsorption compared with organic compounds.

However the investigated polyesters of this present discussion were also expected to behave in the same trend with a maximum inhibition efficiency of 77.63% in case of PGSE at an optimised concentration of 1000 ppm. But the observed inhibition efficiencies are not appreciable which could be reasoned due to the absence of aromatic sites and heteroatoms like sulphur, nitrogen or phosphorous which are the main key factors in rendering good inhibition efficiency. Keen observation of the structure of the synthesised polyesters possessed similar back bone with a difference of methylene spacers. These methylene spacers has increased chain flexibility and segmental motion resulting in a decreased surface coverage which could be due to the absence of flat orientation of the polyesters on the mild steel surface. However the observed moderate inhibition efficiency was due to the +I effect of the $–CH_2$ moieties present.

Based on the above explanation, the order of inhibition efficiencies of the studied polyesters could be arranged in the following sequence.

PGSE > PGAZ > PGSU > PGP > PGA > PGG > PGS > PGM.

This sequence coincides well with the adopted techniques such as weight loss method, impedance and polarisation techniques as explained in the previous sections.

3.4 CONCLUSIONS

The following conclusions were drawn from the above investigations

(i) The studied polyesters were found to be moderate inhibitors for mild steel in 0.5 M H_2SO_4 medium resulting in a maximum inhibition efficiency of 77.63% for PGSE and minimum of 56.64% for PGM.

(ii) Increased inhibition efficiency with concentration and decreased inhibition efficiency with temperature was noticed.

(iii) The weight loss method carried out at a temperature range of 303 K – 333 K led to the calculation of thermodynamic and activation parameters.

(iv) From the various adsorption isotherms studied, the best fit was observed with Langmuir adsorption isotherm.

(v) Physisorption mode of adsorption was predicted from ΔG^o values.

(vi) Impedance measurements were associated with increased charge transfer resistance resulting in the similar trend as observed for weight loss method.

(vii) From the potentiodynamic polarisation curves, mixed type of inhibition was revealed based on E_{corr} values.

(viii) All the measurements carried out were additionally supported by the morphological examination done by adopting FT-IR, XRD, SEM-EDS, AFM and XPS techniques which proved the formation of surface barrier thereby retarding corrosion process.

REFERENCES

1. H. Cang, Z. Fei, J. Shao, W. Shi, Q. Xu, Int. J. Electrochem. Sci., **8** (2013) 720-734.
2. A.A. Al-Amiery, A.A.H. Kadhum, A.B. Mohamad, S. Junaedi, Mater., **6** (2013) 1420-1431.
3. M. Dudukcu, G. Avc, Prog. Org. Coat., **97** (2016) 110-114.
4. A.A.F. Sabirneeza, S. Subhashini, Int. J. ind. Chem., **5** (2014) 111-120.
5. N. B. Rithin Kumar, B. M. Praveen, V. Crasta, J. Bio. Tribo. Corros., **3(46)** (2017) 1-10.
6. M. Mobin, M. Rizvi, L.O. Olasunkanmi, E.E Ebenso, *ACS Omega.*, **2(7)** (2017) 3997-4008.
7. A. Biswas, S. Pal, G. Udayabhanu, Appl. Surf. Sci., **353** (2015) 173-183.
8. M. Mobin, M. A. Khan, M. Parveen, J. Appl. Polym. Science., **121(3)** (2011) 1558-1565.
9. B.D.B. Tiu, R.C. Advincula, React. Funct. Polym., **95** (2015) 25-45.
10. G. Liu, M. Xue, H. Yang, Desalination., **419** (2017) 133-140.
11. R. Karthikaiselvi, S. Subhashini, Arabian J. Chem., **10(1)** (2017) s627-s635.
12. A.F.S. Abdul Rahiman, S. Sethumanickam, Arabian J. Chem., **10(2)** (2017) s3358-s3366.
13. Y. Zhang, Y. Shao, X. Liu, C. Shi, Y. Wang, G. Meng, X. Zeng, Y. Yang, Prog. Org. Coat., **111** (2017) 240-247.
14. A. Biswas, P. Mourya, D. Mondal, S. Pal, G. Udayabhanu, J. Mol. Liq., **251** (2018) 470-479.
15. G. Nirmala Devi, J. Saranya, A. Kiruthika, L.O. Olasunkanmi, E.E. Ebenso, S. Chitra, J. Mol. Liq., **232** (2017) 9-19.
16. N.K. Gupta, P.G. Joshi, V. Srivastava, M.A. Quraishi, Int. J. Biol. Macromol., **106** (2018) 704-711.
17. A. El Jaouhari, A. El Asbahani, M. Bouabdallaoui, Z. Aouzal, D. Filotás, E.A. Bazzaoui, L. Nagy, G. Nagy, M. Bazzaoui, A. Albourine, D. Hartmann, Synth. Met., **226** (2017) 15-24.
18. M.M. El-Deeb, S.M. Sayyah, S.S. Abd El-Rehim, S.M. Mohamed, Arabian J. Chem., **8** (2015) 527-537.
19. I.B. Obot, I.B. Onyeachu, A. Madhan Kumar, Carbohydr. Polym., **178** (2017) 200-208.
20. M. Mobin, M. Rizvi, Carbohydr. Polym., **160** (2017) 172-183.

21. G. Nirmala Devi, J. Saranya, N. Manjubaashini, T.D. Thangadurai, S.M. Roopan, S. Chitra, Prog. Org. Coat., **109** (2017) 117-125.
22. A. Zhu, H. Wang, C. Zhang, M. Rui, C. Zhou, C. Chen, Prog. Org. Coat., **112** (2017) 109-117.
23. P. Sounthari, A. Kiruthika, J. Saranya, K. Parameswari, S. Chitra, Ecotoxicol. Environ. Saf., **134** (2016) 319-326.
24. C. Japu, A. Martínez, D. IIarduya, A. Alla, S. Munoz-Guerra, Polym., **55(10)** (2014) 2294-2304.
25. G. Totaro, L. Cruciani, M. Vannini, G. Mazzola, D.D. Gioia, A. Celli, L. Sisti, Eur. Polym. J., **56** (2014) 174-184.
26. I.C. Yeha, B.C. Rinderspacher, J.W. Andzelma, L.T. Curetonb, J.L. Scala, Polym., **55(1)** (2014) 166-174.
27. Z. You, H. Cao, J. Gao, P.H. Shin, B.W. Day, Y. Wang, Biomaterials., **31** (2010) 3129-3138.
28. S.W. Fang, P.D. Caro, P.Y. Pennarun, C. Vaca-Garcia, S. Thiebaud-Roux, Ind. Crops Prod., **43** (2013) 398-404.
29. Patel, A.K. Gaharwar, G. Iviglia, H. Zhang, S. Mukundan, S.M. Mihaila, D. Demarchi, A. Khademhosseini, Biomaterials., **34(16)** (2013) 3970-3983.
30. R. Rai, M. Tallawi, J.A. Roether, R. Detsch, N. Barbani, E. Rosellini, J. Kaschta, D.W. Schubert, A.R. Boccaccini, Mater. Lett., **105** (2013) 32-35.
31. M. Agach, S. Delbaere, S. Marinkovic, B. Estrine, V.N. Rataj, *Colloids Surf., A Physicochem* Eng Asp., **419** (2013) 263-273.
32. V.M. Weiss, T. Naolou, G. Hause, J. Kuntsche, J. Kressler, K. Mader, J. Control. Release., **158(1)** (2012) 156-164.
33. J. Scheirs, T.E. Long, Modern polyesters: chemistry and technology of polyesters and copolyesters, John Wiley & Sons, Hoboken, (2003).
34. M. Srivastava, P. Tiwari, S.K. Srivastava, R. Prakash, J. Gopal, J. Mol. Liq., **236** (2017) 184-197.
35. A. Paul, K.J. Thomas, V.P. Raphael, K.S. Shaju, J. Appl. Chem., **1(6)** (2012) 17-23.
36. I.A. Akpan , N.A.O. Offiong, Int. J. corros., **2013** (2013) 1-5.
37. S. Subhashini, A.A.F. Sabirneeza, Proc. World congr. Eng. Comput. Sci., **2** (2011) 1-6.
38. L. Khandelwal, C.B. Verma, M.A. Quraishi, J. Mater. Environ. Sci., **6(3)** (2015) 810-817.

39. R. Karthikaiselvi, S. Subhashini, J. Assn. Arab. Univ. Basic. Appl. Sci., **16** (2014) 74-82.
40. V.N. Sheeja, S. Subhashini, Int. J. Sci. Eng. Technol. Res., **4(6)** (2015) 2146-2151.
41. M.P.Chakravarthy, K.N.Mohana, ISRN Corros., **2014** (2014) 1-13.
42. A.S. Fouda, M.A. Elmorsi, A. Elmekkawy, Afr. J. *Pure* Appl. Chem., **7(10)** (2013) 337-349.
43. M.N. Idris, A.R. Dud, N.K. Othman, A. Jalar, Int. J. Eng. Technol., **13(3)** (2013) 47-51.
44. H. Elmsellem, A. Aouniti,Y. Toubi, H. Steli, M. Ellazouzi, S. Radi, B. Elmahi, Y. Elouadi, A. Chetaouani, B. Hammaouti, Der pharma chem., **7(7)** (2015) 353-364.
45. Y. EL Aoufir, H. Lgaz, K. Toumiat, R. Salghi, S. Jodeh, M. Zougagh, A. Guenbour, H. Oudda, Res. J. Pharm. Biol. Chem. Sci., **7(5)** (2016) 1200-1208.
46. B.M. Ministry, N.S. Patel, S. Sahoo, S. Jauhari, Bull. Mater. Sci., **35(3)** (2012) 459-469.
47. A. Paul, K.J. Thomas, V.P. Raphael, K.S. Shaju, ISRN Corros., **2012** (2012) 1-9.
48. J. Saranya, P. Sounthari, K. Parameswari, S. Chitra, Der pharma chem., **7(8)** (2015) 187-196.
49. H. Tayebi, H. Bourazmi, B. Himmi, A. El Assyry, Y. Ramli, A. Zarrouk, A. Geunbour, B. Hammouti, E.E. Ebenso, Pharm Lett ., **6(6)** (2014) 20-34.
50. F.M. Mahgoub, S.M. Al-Rashdi, Open J Phys Chem., **6** (2016) 54-66.
51. A.Y.I. Rubaye, H.T. Abdulsahib, A.A. Abdulwahid., J. Encaps. Ads. Sci., **5** (2015) 155-164.
52. A.A. Al-Amiery, A.A.H. Kadhum, A. Kadihum, A.B. Mohamad, C.K. How, S. Junaedi, Mater., **7** (2014) 787-804.
53. B. M. Prasanna, B.M. Praveen, N. Hebbar, T.V. Venkatesha, H.C. Tando, Int. J. Ind. Chem., **7(1)** (2016) 9-19.
54. H. Cang, Z. Fei, J. Shao, W. Shi, Q. Xu, Int.J. Electrochem. Sci., **8** (2013) 720-734.
55. K.R. Ansari, R. Sowmya, D. Nalini, M.A. Quraishi, Congent. Chem. Mater. Sci., **2(1)** (2016) 1-15.
56. N. Antony, H.B. Sherine, S. Rajendran, The Arabian J. Sci. Eng., **35** (2010) 43-53.
57. Y. Abboud, O. Tanane, A. El Bouari, R. Salghi, B. Hammouti, A. Chetouani, S. Jodeh, Corros. Eng. Sci. Technol., **51** (2016) 557-565.
58. A.M. Alsabagh , M.A. Migahed, H.S. Awad, Corr. Sci., **48** (2006) 813-828.
59. Pal, S. Dey, D. Sukul, Res. Chem. Interm., **42** (2016) 4531-4549.

60. M.M. Solomon, S.A. Umoren, J. Colloid. Interface. Sci., **462** (2016) 29-41.
61. Y. Qiang, L. Guo, Sci. rep., **6** (2016) 1-14.
62. A.R. González-Elipe, A. Martinez-Alonso, J.M.D. Tascon, Surf. Interface. Anal., **12(12)** (1988) 565–571.
63. R.D. Boyd, J. Verran, K.E. Hall, C. Underhill, S. Hibbert, R. West, Appl. Surf. Sci., **172(1-2)** (2001) 135-143.
64. A.G. Kannan, N.R. Choudhury, N.K. Dutta, Polym., **48** (2007) 7078–7086.
65. Priyanka Singh, Vandana Srivastava, M.A. Quraishi, J. Mol. Liq., **216** (2016) 164-173.
66. A. Dandia, S.L. Gupta, P. Singh, M.A. Quraishi, ACS Sustainable Chem. Eng., **1(10)** (2013) 1303–1310.

Table 3.1 Inhibition efficiencies of various concentrations of the aliphatic polyesters for corrosion of mild steel in 0.5 M H_2SO_4 by weight loss measurement at ± 303 K

Name of the Inhibitor	Conc. (ppm)	Weight loss (g)	Inhibition Efficiency (%)	Surface Coverage (θ)	Corrosion rate (g cm^{-2} hr^{-1})
BLANK		0.2015	-	-	19.97
PGM	10	0.1188	41.07	0.4107	11.77
	50	0.1124	44.21	0.4421	11.14
	100	0.111	44.85	0.4485	11.01
	500	0.1050	47.89	0.4789	10.41
	1000	0.0874	56.64	0.5664	8.66
	1500	0.0886	56.01	0.5601	8.78
PGS	10	0.1132	43.81	0.4381	11.22
	50	0.1109	44.98	0.4498	10.99
	100	0.1107	45.07	0.4507	10.97
	500	0.0923	54.21	0.5421	9.14
	1000	0.0859	57.35	0.5735	8.52
	1500	0.0864	57.11	0.5711	8.56
PGG	10	0.1119	44.48	0.4448	11.09
	50	0.1094	45.72	0.4572	10.84
	100	0.1088	46.00	0.4600	10.78
	500	0.0886	56.02	0.5602	8.78
	1000	0.0814	59.61	0.5961	8.07
	1500	0.0842	58.23	0.5823	8.34
PGA	10	0.1031	48.82	0.4882	10.22
	50	0.1009	49.92	0.4992	10.00
	100	0.0975	51.63	0.5163	9.66
	500	0.0884	56.12	0.5612	8.76
	1000	0.0783	61.14	0.6114	7.76
	1500	0.0806	60.01	0.6001	7.98

PGP	10	0.1026	49.07	0.4907	10.17
	50	0.0981	51.32	0.5132	9.72
	100	0.0944	53.15	0.5315	9.36
	500	0.0834	58.61	0.5861	8.27
	1000	0.0774	61.60	0.6160	7.67
	1500	0.0777	61.44	0.6144	7.70
PGSU	10	0.0985	51.13	0.5113	9.76
	50	0.0977	51.51	0.5151	9.68
	100	0.0932	53.76	0.5376	9.23
	500	0.0818	59.41	0.5941	8.10
	1000	0.0736	63.47	0.6347	7.30
	1500	0.0749	62.81	0.6281	7.42
PGAZ	10	0.0976	51.59	0.5159	9.67
	50	0.0934	53.66	0.5366	9.25
	100	0.0929	53.88	0.5388	9.21
	500	0.0756	62.49	0.6249	7.49
	1000	0.0645	67.97	0.6797	6.40
	1500	0.0699	65.32	0.6532	6.92
PGSE	10	0.0956	52.55	0.5255	9.48
	50	0.0923	54.18	0.5418	9.15
	100	0.0919	54.38	0.5438	9.11
	500	0.0723	64.14	0.6414	7.16
	1000	0.0451	77.63	0.7763	4.47
	1500	0.0628	68.84	0.6884	6.22

Table 3.2 Inhibition efficiencies of selected concentrations of the aliphatic polyesters for corrosion of mild steel in 0.5 M H_2SO_4 by weight loss measurement at higher temperature

Name of the inhibitor	Conc. (ppm)	303 K		313 K		323 K		333 K	
		IE (%)	CR (g cm^{-2} hr^{-1})	IE (%)	CR (g cm^{-2} hr^{-1})	IE (%)	CR (g cm^{-2} hr^{-1})	IE (%)	CR (g cm^{-2} hr^{-1})
BLANK	-	-	17.39	-	80.13	-	102.01	-	122.34
PGM	10	34.02	11.48	30.21	55.92	26.43	75.05	21.08	96.55
	100	36.92	10.97	33.2	53.52	29.43	71.99	24.58	92.27
	1000	51.11	8.50	43.98	44.89	37.85	63.40	31.74	83.51
PGS	10	36.24	11.09	32.89	53.77	29.96	71.45	25.42	91.24
	100	39.49	10.52	35.64	51.57	31.96	69.41	26.63	89.76
	1000	53.68	8.06	48.57	41.21	42.95	58.20	37.55	76.40
PGG	10	37.61	10.85	35.12	51.99	31.25	70.13	28.93	86.95
	100	40.17	10.41	36.02	51.26	33.69	67.64	28.59	87.37
	1000	55.56	7.73	53.11	37.57	47.85	53.20	41.77	71.24
PGA	10	40.00	10.44	37.81	49.83	33.52	67.82	30.97	84.45
	100	42.22	10.05	40.83	47.41	36.57	64.70	32.19	82.96
	1000	56.75	7.52	54.53	36.43	51.61	49.36	46.86	65.01
PGP	10	41.54	10.17	38.35	49.40	36.43	64.85	31.91	83.30
	100	46.15	9.37	43.32	45.42	39.94	61.27	35.81	78.53
	1000	58.29	7.25	56.98	34.47	54.68	46.23	51.05	59.89
PGSU	10	42.74	9.96	40.28	47.85	37.89	63.36	34.56	80.06
	100	47.52	9.13	45.65	43.55	42.29	58.87	39.57	73.93
	1000	59.66	7.02	57.52	34.04	55.91	44.98	53.22	57.23
PGAZ	10	44.44	9.66	42.09	46.40	40.23	60.97	36.8	77.32
	100	49.23	8.83	46.11	43.18	45.06	56.04	42.29	70.61
	1000	62.39	6.54	60.09	31.98	57.36	43.50	55.25	54.75
PGSE	10	46.50	9.31	43.96	44.90	41.68	59.49	39.21	74.37
	100	55.04	7.82	51.52	38.85	48.36	52.68	45.58	66.58
	1000	66.15	5.89	63.72	29.07	60.81	39.98	58.43	50.86

Table 3.3 Activation parameters for mild steel corrosion in 0.5 M H_2SO_4 calculated by Arrhenius, Transition State and basic thermodynamic equations

Name of the inhibitor	Ea kJ/ mol	ΔH^o kJ / mol	ΔS^o kJ /mol / K	ΔG^o (kJ / mol)			
				303	313	323	333
Blank	51.81	49.17	-55.99	17.01	17.57	18.14	18.69
PGM	61.10	58.46	-31.23	9.52	9.83	10.14	10.45
PGS	60.21	57.56	-34.70	10.57	10.92	11.26	11.61
PGG	59.46	56.82	-34.64	11.46	11.83	12.21	12.59
PGA	57.49	54.86	-44.30	13.47	13.92	14.35	14.81
PGP	56.25	53.61	-48.72	14.82	15.3	15.79	16.27
PGSU	55.85	53.21	-50.25	15.28	15.78	16.28	16.78
PGAZ	56.74	54.10	-47.86	14.55	15.03	15.51	15.99
PGSE	57.64	55	-45.77	13.92	14.38	14.83	15.29

Table 3.4 Langmuir adsorption isotherm parameters for mild steel in 0.5 M H_2SO_4 containing various concentrations of the aliphatic polyesters at room temperature

Name of the inhibitor	Slope	K	R^2	$-\Delta G^o_{ads}$ kJ mol^{-1}
PGM	1.76	38.38	0.9951	36.71
PGS	1.72	30.63	0.9987	36.15
PGG	1.66	32.28	0.9985	36.28
PGA	1.63	25.70	0.9976	35.70
PGP	1.61	19.89	0.9992	35.05
PGSU	1.57	22.71	0.9986	35.39
PGAZ	1.48	24.86	0.9985	35.90
PGSE	1.44	25.76	0.9984	35.71

Table 3.5 Temkin adsorption isotherm parameters for mild steel in 0.5 M H_2SO_4 containing various concentrations of the aliphatic polyesters at room temperature

Name of the inhibitor	Slope	K	R^2	$-\Delta G^o_{ads}$ kJ mol^{-1}	a
PGM	0.07	0.3294	0.9227	24.73	14.93
PGS	0.06	0.3558	0.8956	24.81	16.66
PGG	0.07	0.3643	0.9507	24.77	14.93
PGA	0.06	0.4165	0.8998	25.43	16.66
PGP	0.05	0.4224	0.9696	25.38	20
PGSU	0.05	0.4331	0.8998	25.50	20
PGAZ	0.07	0.4202	0.9163	25.25	14.93
PGSE	0.08	0.4228	0.9186	24.98	12.5

Table 3.6 El-Awady adsorption isotherm parameters for mild steel in 0.5 M H_2SO_4 containing various concentrations of the aliphatic polyesters at room temperature

Name of the inhibitor	Slope	K	R^2	ΔG^o_{ads} kJ mol^{-1}	1/y
PGM	0.1173	-0.29	0.7479	10.63	8.52
PGS	0.1258	-0.27	0.8021	10.56	8.33
PGG	0.1408	-0.28	0.8061	10.59	7.14
PGA	0.1051	-0.15	0.8339	9.93	9.09
PGP	0.1126	-0.6	0.9398	9.88	9.09
PGSU	0.1127	-0.13	0.8344	9.74	9.09
PGAZ	0.1486	-0.17	0.8164	10.01	6.66
PGSE	0.2246	-0.26	0.6498	10.53	4.54

Table 3.7 Flory Huggins adsorption isotherm parameters for mild steel in 0.5 M H_2SO_4 containing various concentrations of the aliphatic polyesters at room temperature

Name of the inhibitor	Slope	K	R^2	$-\Delta G^o_{ads}$ kJ mol^{-1}	1/a
PGM	12.66	1.1024	0.6689	27.77	0.0789
PGS	12.36	1.2682	0.7648	28.12	0.0809
PGG	10.69	0.9125	0.7651	27.29	0.0935
PGA	14.16	2.3926	0.7942	29.72	0.0706
PGP	14.38	2.6436	0.9185	29.97	0.0695
PGSU	12.75	2.2309	0.8031	29.54	0.0784
PGAZ	8.91	1.0796	0.7721	27.71	0.1122
PGSE	4.35	-0.4751	0.5519	25.65	0.2298

Table 3.8 Thermodynamic parameters for mild steel corrosion in 0.5 M H_2SO_4 at different temperatures calculated from van't Hoff and Gibbs Helmholtz equation

Name of the inhibitor	Van't Hoff equation		Gibbs-Helmholtz equation	$-\Delta G^o_{ads}$ kJ mol^{-1}			
	ΔH^o_{ad} skJ mol^{-1}	ΔS^o_{ads} kJ mol^{-1}	ΔH^o_{ads} kJ mol^{-1}	303 K	313 K	323 K	333 K
PGM	-22.51	0.0169	-22.51	27.63	27.8	28.01	28.12
PGS	-18.39	0.0314	-18.39	27.89	28.28	28.57	28.84
PGG	-15.65	0.0414	-15.64	28.08	28.75	29.11	29.33
PGA	-10.94	0.0572	-10.93	28.20	28.90	29.51	29.90
PGP	-8.09	0.0671	-8.09	28.37	29.16	29.84	30.36
PGSU	-7.13	0.0706	-7.13	28.51	29.22	29.97	30.61
PGAZ	-8.37	0.0674	-8.36	28.8	29.49	30.14	30.83
PGSE	-9.35	0.0656	-9.34	29.21	29.89	30.51	31.19

Table 3.9 AC-impedance parameters for the corrosion of mild steel for selected concentrations of the aliphatic polyesters in 0.5 M H_2SO_4

Name of the inhibitor	Conc. (ppm)	R_{ct} (ohm cm^2)	Cdl (µF/cm^2)	Inhibition efficiency (%)
BLANK	-	15.8	21.5	-
PGM	10	18.2	15.7	13.19
	100	24.3	14.1	34.98
	1000	26.4	12.9	40.15
PGS	10	20.1	13.7	21.39
	100	27.2	13.5	41.91
	1000	28.9	12.1	45.33
PGG	10	24.3	12.6	34.98
	100	28.4	12.2	44.37
	1000	32.6	11.6	51.53
PGA	10	26.7	12.5	40.82
	100	29.8	11.1	46.98
	1000	34.4	10.1	54.07
PGP	10	29.9	16.7	47.16
	100	33.1	15.2	52.27
	1000	37.5	14.3	57.87
PGSU	10	29.9	15.8	47.16
	100	34.2	15.2	53.80
	1000	41.1	14.8	61.56
PGAZ	10	30.1	18.7	47.51
	100	35.2	18.4	55.11
	1000	43.6	14.9	63.76
PGSE	10	30.9	19.8	48.87
	100	37.3	18.5	57.64
	1000	48.5	16.8	67.42

Table 3.10 Potentiodynamic polarisation parameters for corrosion of mild steel with selected concentration of the aliphatic polyesters in 0.5 M H_2SO_4

Name of the inhibitor	Conc. (ppm)	Tafel slopes (mV/dec)		-Ecorr (mV) vs SCE	I_{corr} ($\mu A/cm^2$)	Inhibition efficiency (%)
		b_a	b_c			
BLANK	-	63	153	476.9	896.52	
PGM	10	68	161	479.8	604.43	32.58
	100	69	119	514.5	540.27	39.74
	1000	67	117	528.1	498.23	44.43
PGS	10	60	112	512	530.23	40.86
	100	61	114	508.4	525.27	41.41
	1000	62	113	518.1	489.56	45.39
PGG	10	80	188	515.2	525.36	41.40
	100	72	123	470.3	511.58	42.94
	1000	66	115	524	475.63	46.95
PGA	10	87	185	456.7	526.02	41.33
	100	61	120	501.2	505.45	43.62
	1000	70	115	537.5	490.56	45.28
PGP	10	64	151	497.9	529.31	40.96
	100	63	137	498.8	480.18	46.44
	1000	71	120	519.6	450.41	49.76
PSSU	10	68	125	502.4	498.35	44.41
	100	81	105	526.1	470.51	47.52
	1000	84	114	539.8	440.25	50.89
PGAZ	10	53	139	487.4	468.56	47.74
	100	57	127	493.2	435.69	51.40
	1000	68	118	522	410.25	54.24
PGSE	10	63	136	498.8	440.28	50.89
	100	62	126	492.5	415.28	53.68
	1000	69	111	517.4	342.23	61.83

Table 3.11 Elemental composition from EDS spectra

Element (Wt %)	Blank	PGG inhibited	PGP inhibited
O	31.58	20.85	24.29
S	1.12	4.9	3.94
Fe	64.87	35.41	27.49
C	2.43	38.84	44.28

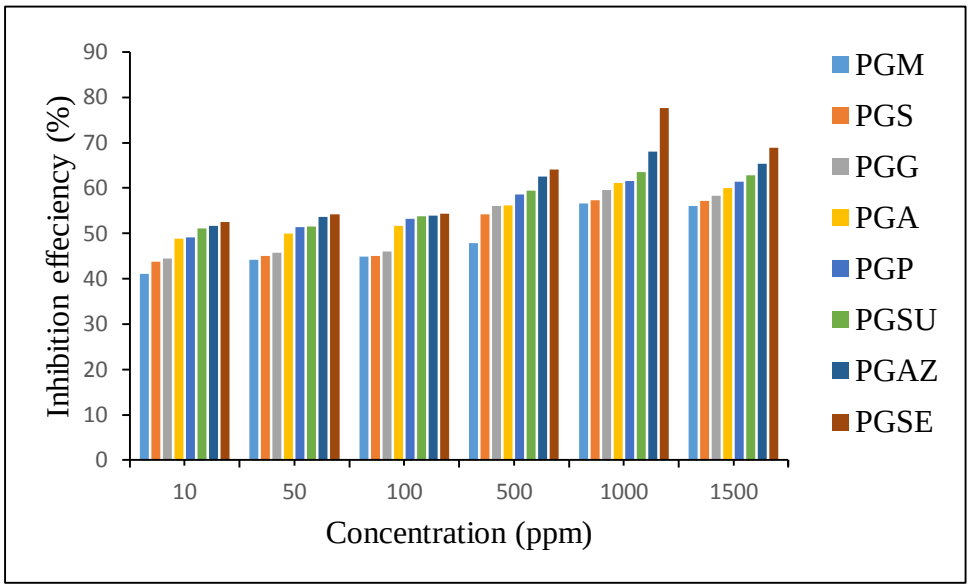

Fig. 3.1 Variation of inhibition efficiency for different concentrations of aliphatic polyesters in 0.5 M H_2SO_4

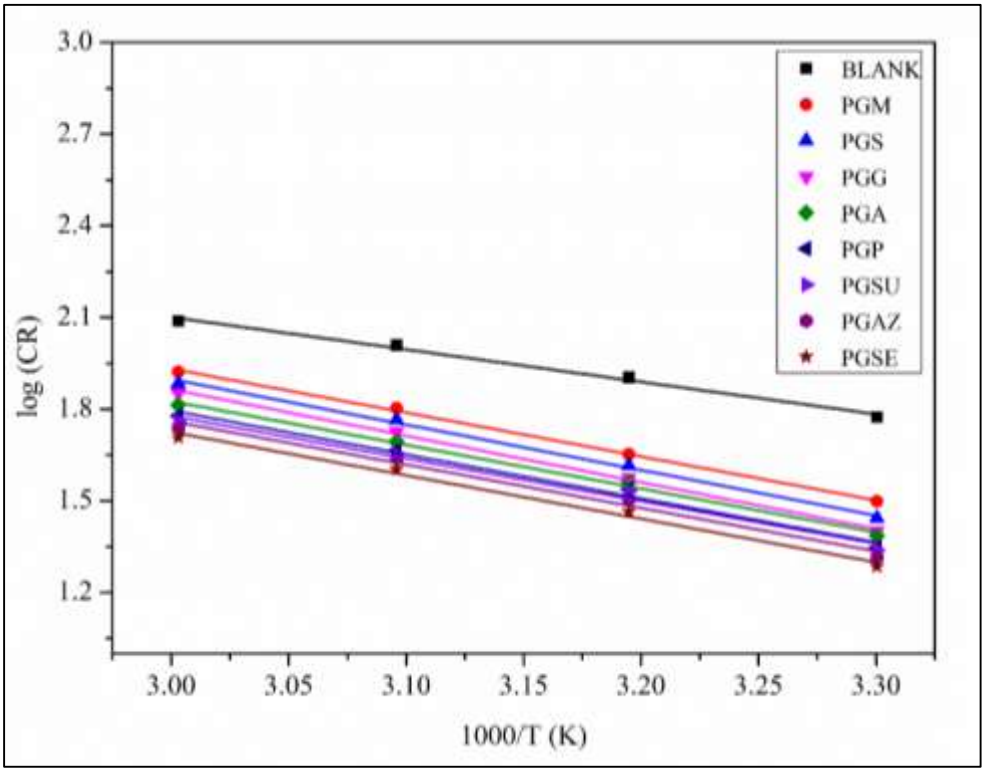

Fig. 3.2 Arrhenius plot for corrosion of mild steel in 0.5 M H_2SO_4 in the absence and presence of aliphatic polyesters

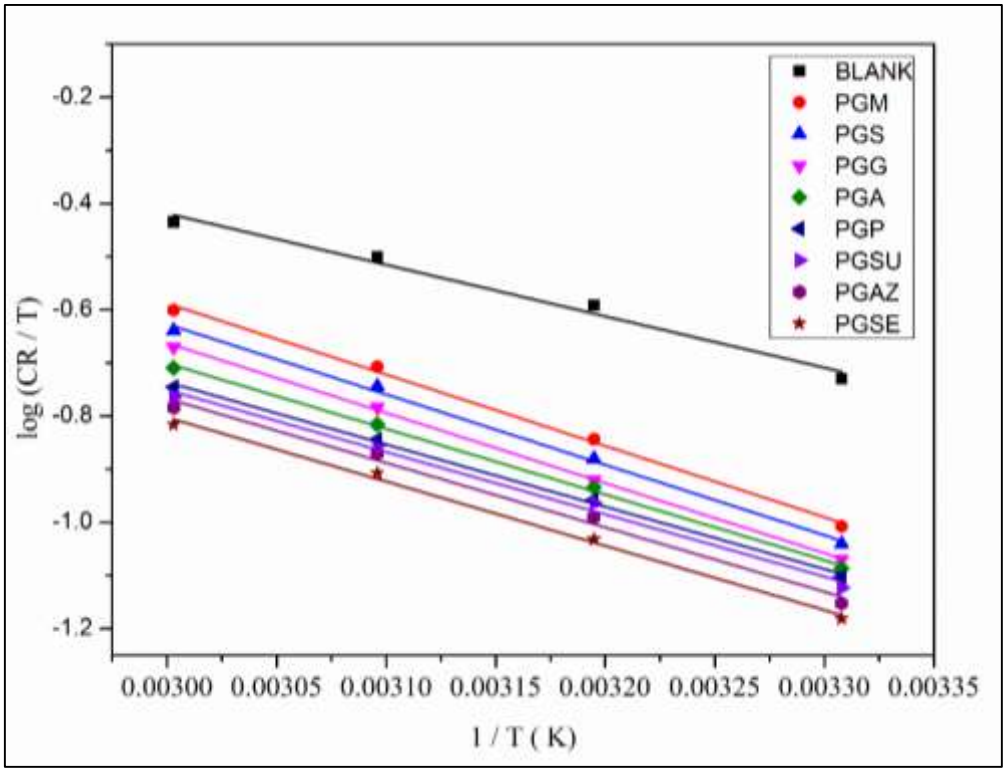

Fig. 3.3 Transition State plot for corrosion of mild steel in 0.5 M H_2SO_4 in the absence and presence of aliphatic polyesters

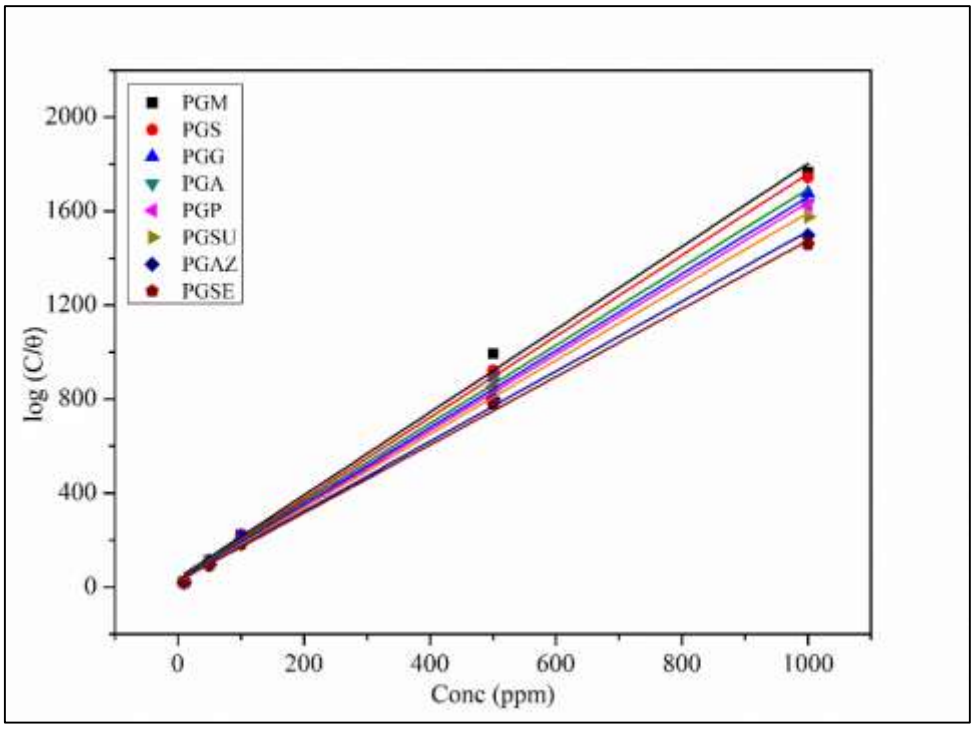

Fig. 3.4 Langmuir plot of corrosion of mild steel in 0.5 M H_2SO_4 in the absence and presence of aliphatic polyesters

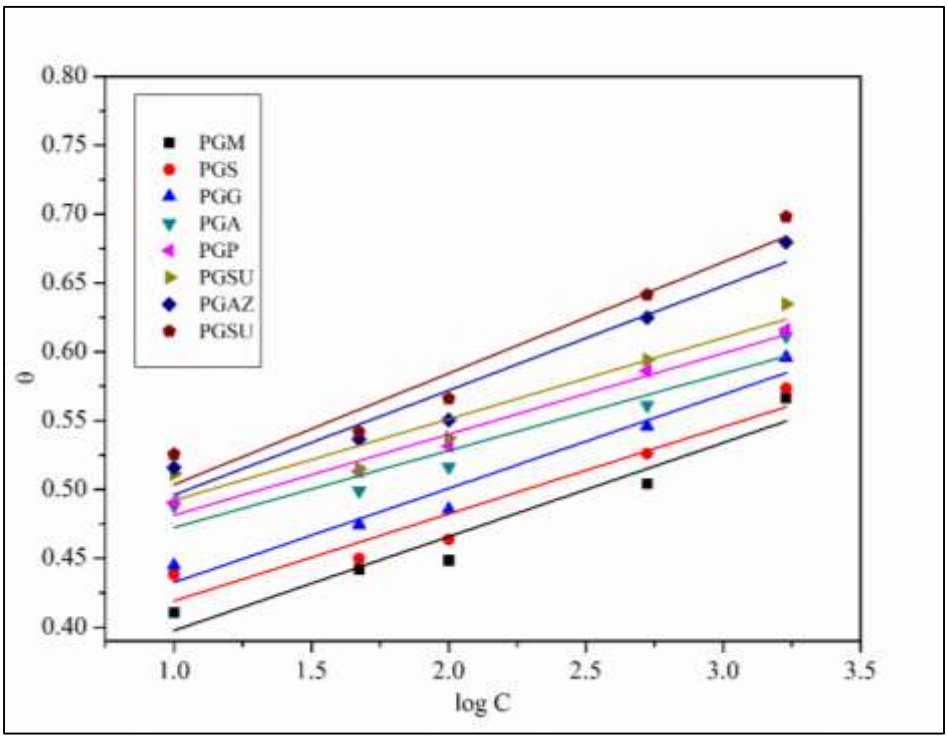

Fig. 3.5 Temkin plot for corrosion of mild steel in 0.5 M H_2SO_4 in the absence and presence of aliphatic polyesters

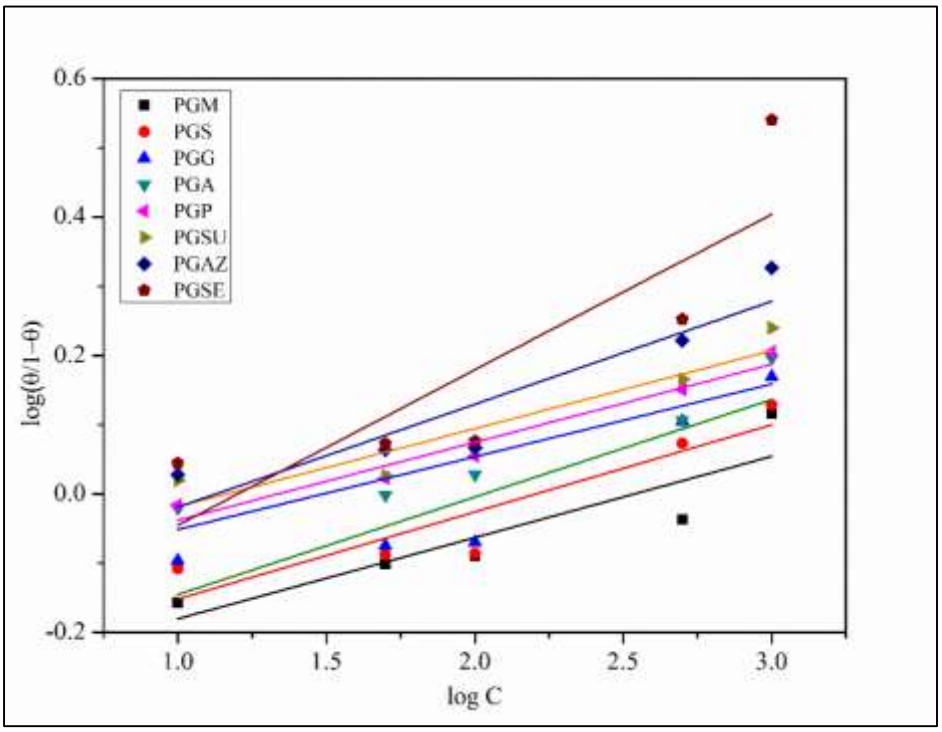

Fig. 3.6 El-Awady plot for corrosion of mild steel in 0.5 M H_2SO_4 in the absence and presence of aliphatic polyesters

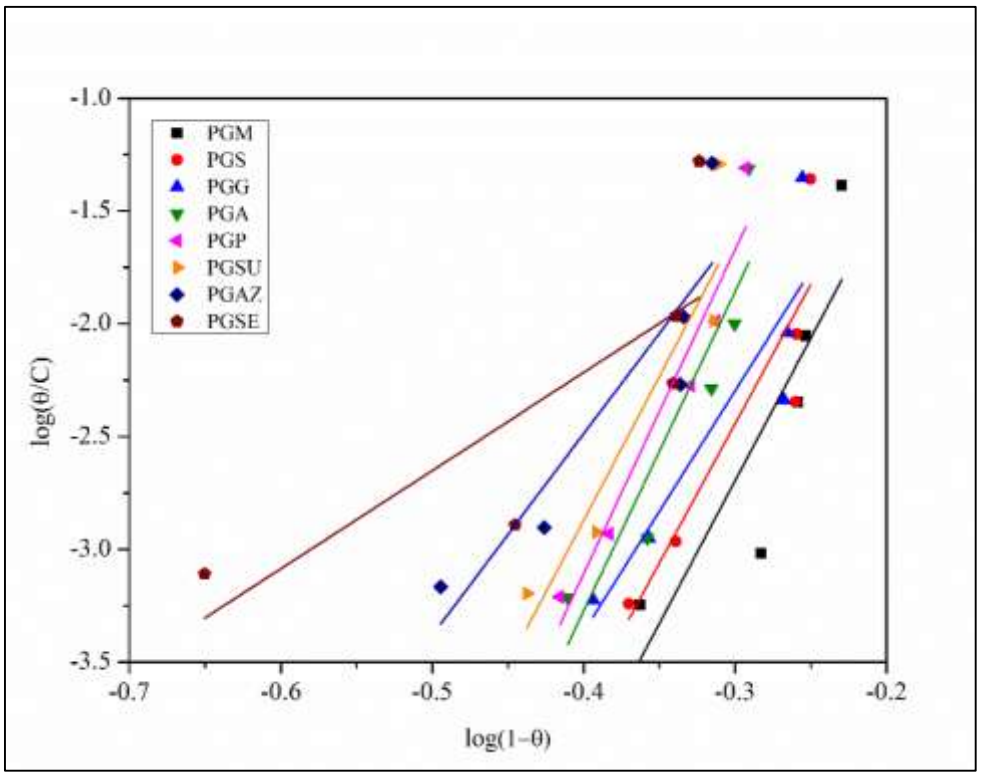

Fig. 3.7 Flory-Huggins plot for corrosion of mild steel in 0.5 M H_2SO_4 in the absence and presence of aliphatic polyesters

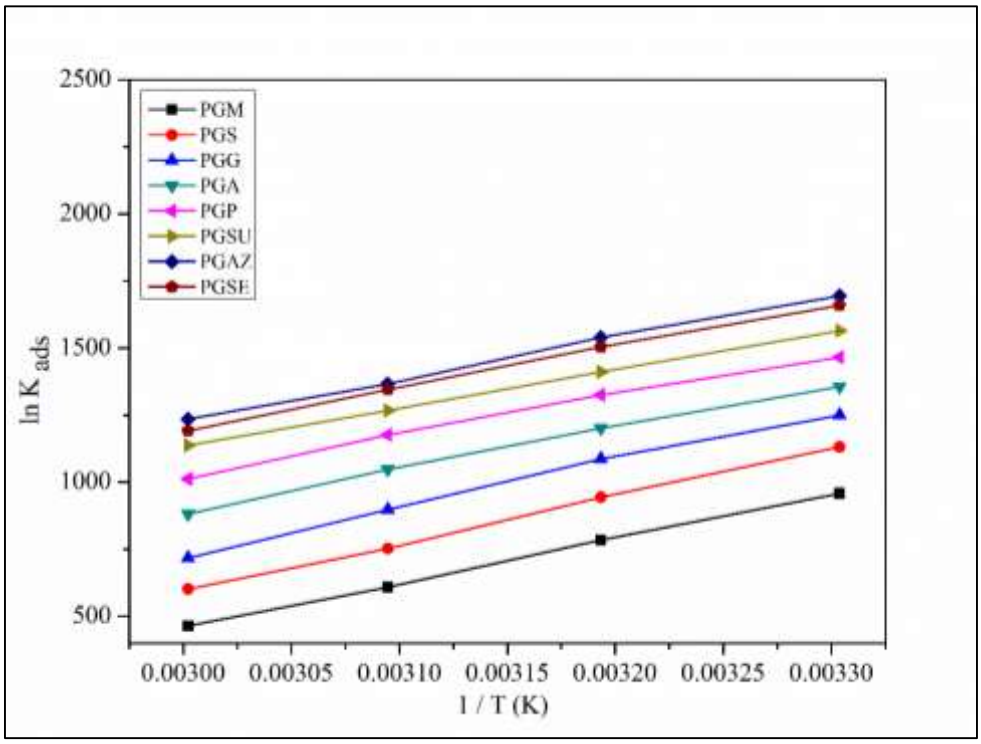

Fig. 3.8 The relationship between log K_{ads} and 1/T

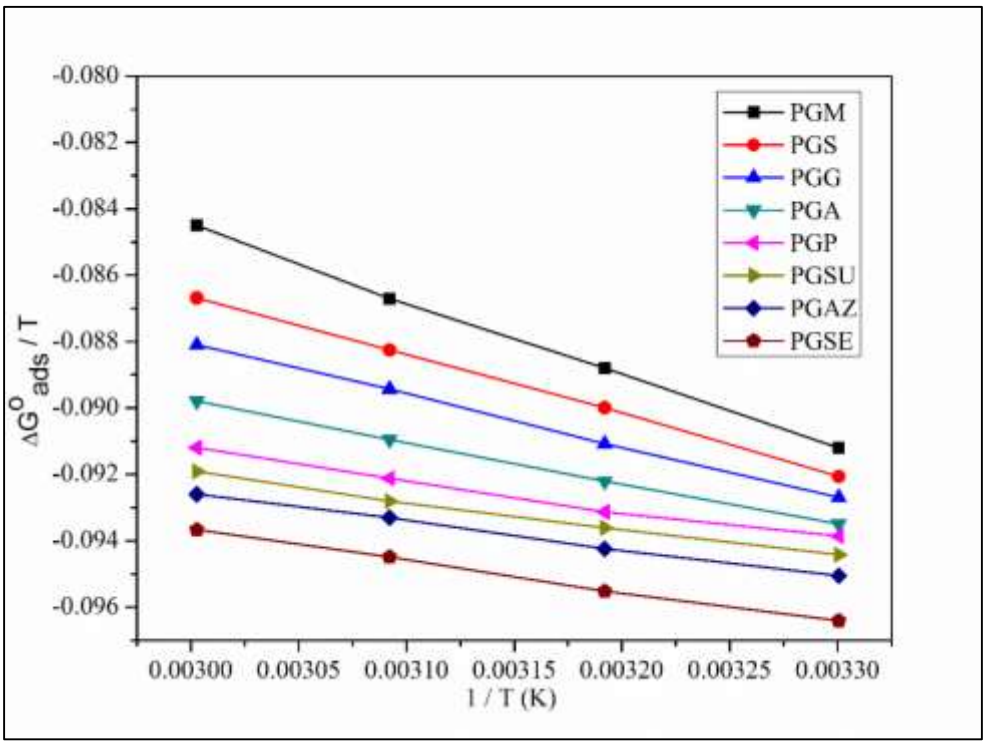

Fig. 3.9 The relationship between $\Delta G^{\circ}_{ads}/T$ and 1/T

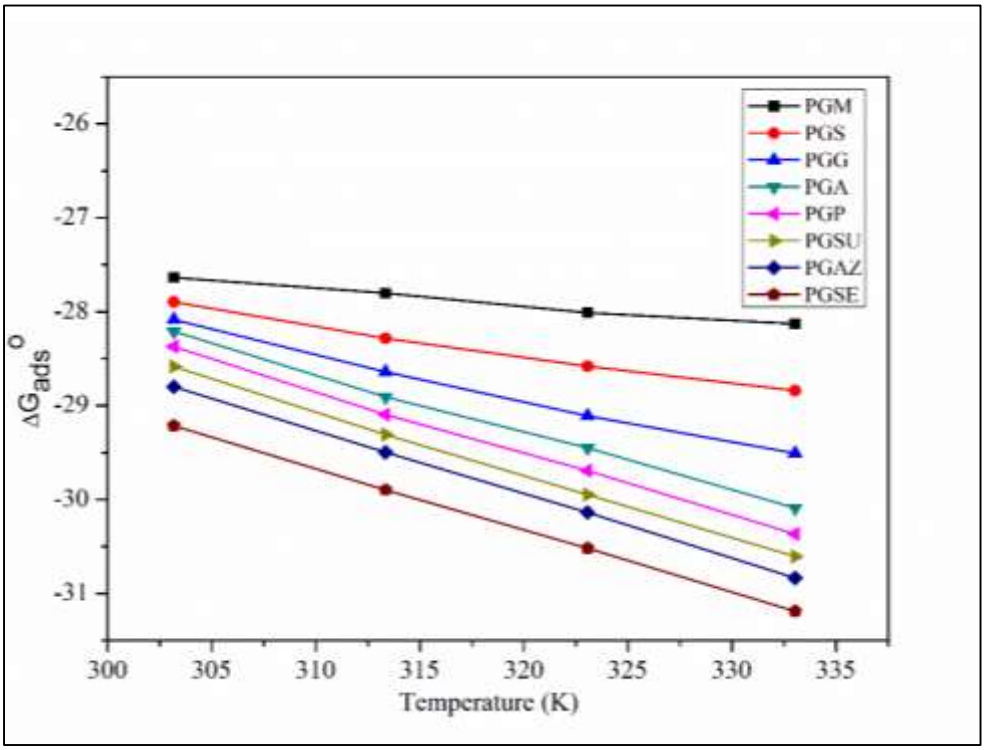

Fig. 3.10 The relationship between ΔG°_{ads} and T

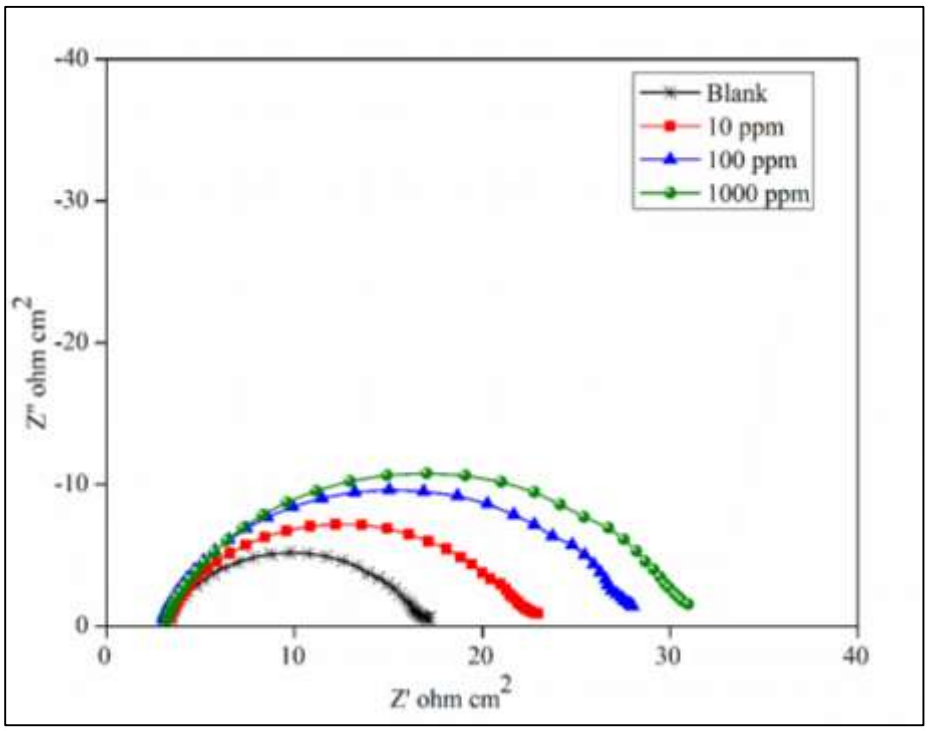

Fig. 3.11 Nyquist plot for mild steel in 0.5 M H_2SO_4 for selected concentrations of PGM

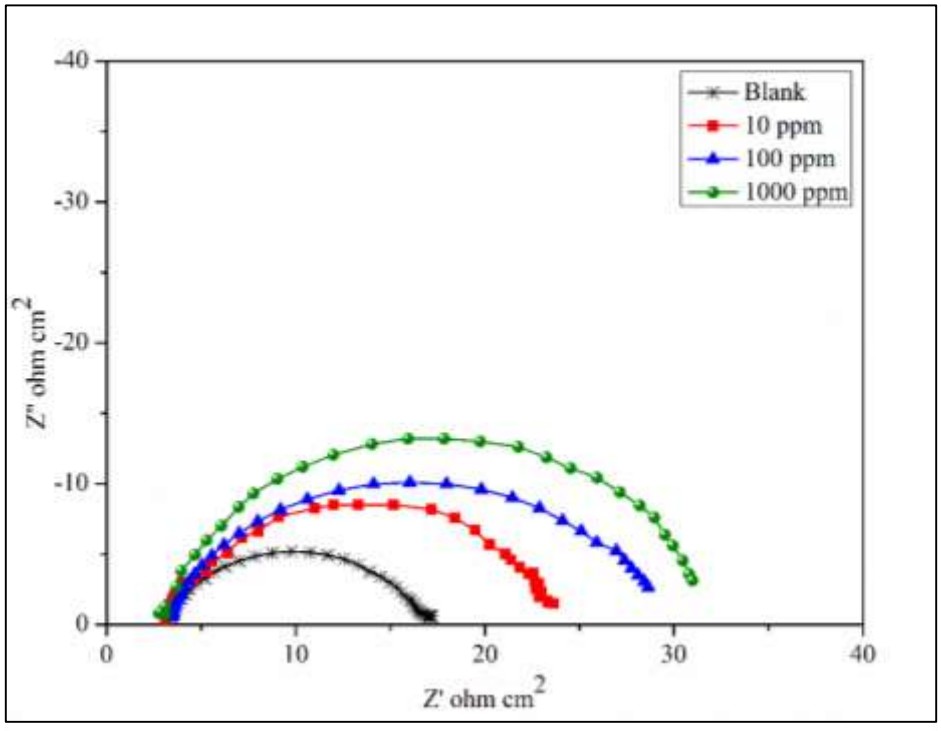

Fig. 3.12 Nyquist plot for mild steel in 0.5 M H_2SO_4 for selected concentrations of PGS

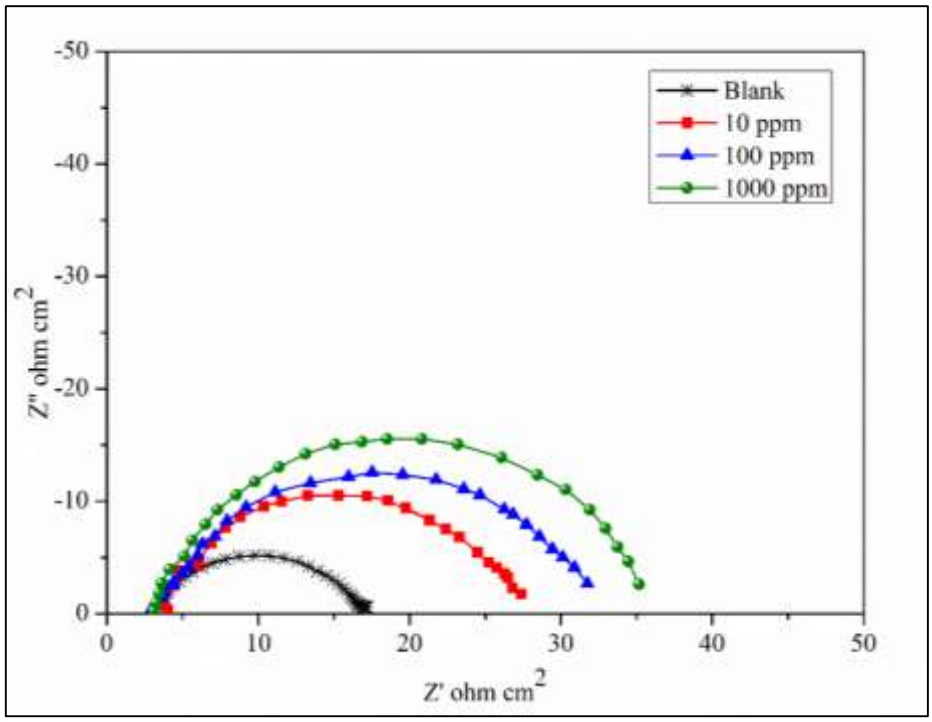

Fig. 3.13 Nyquist plot for mild steel in 0.5 M H_2SO_4 for selected concentrations of PGG

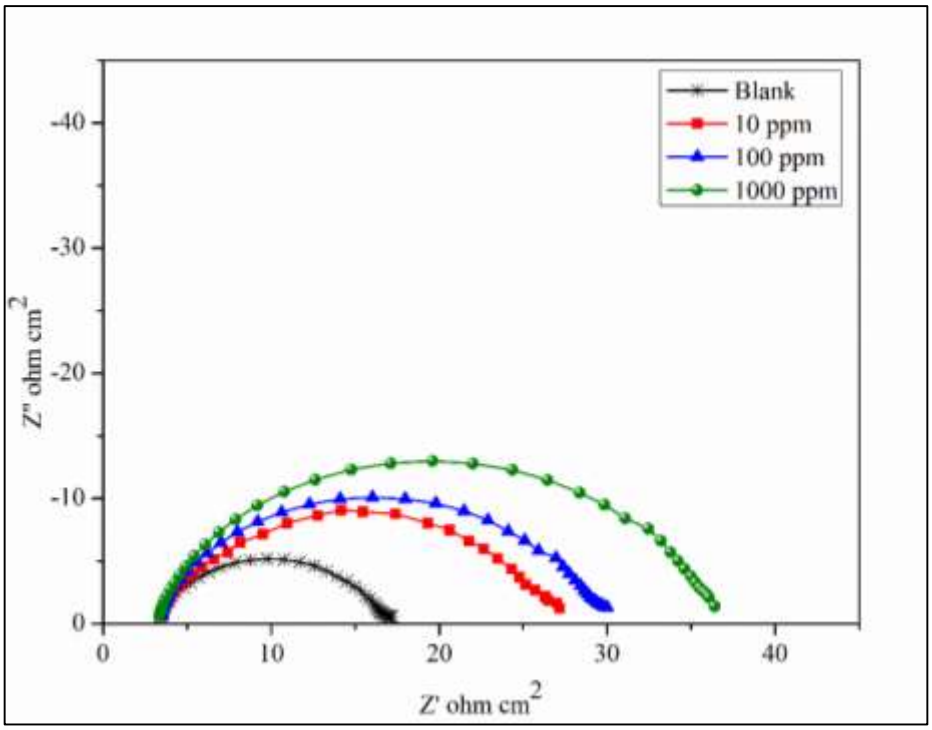

Fig. 3.14 Nyquist plot for mild steel in 0.5 M H_2SO_4 for selected concentrations of PGA

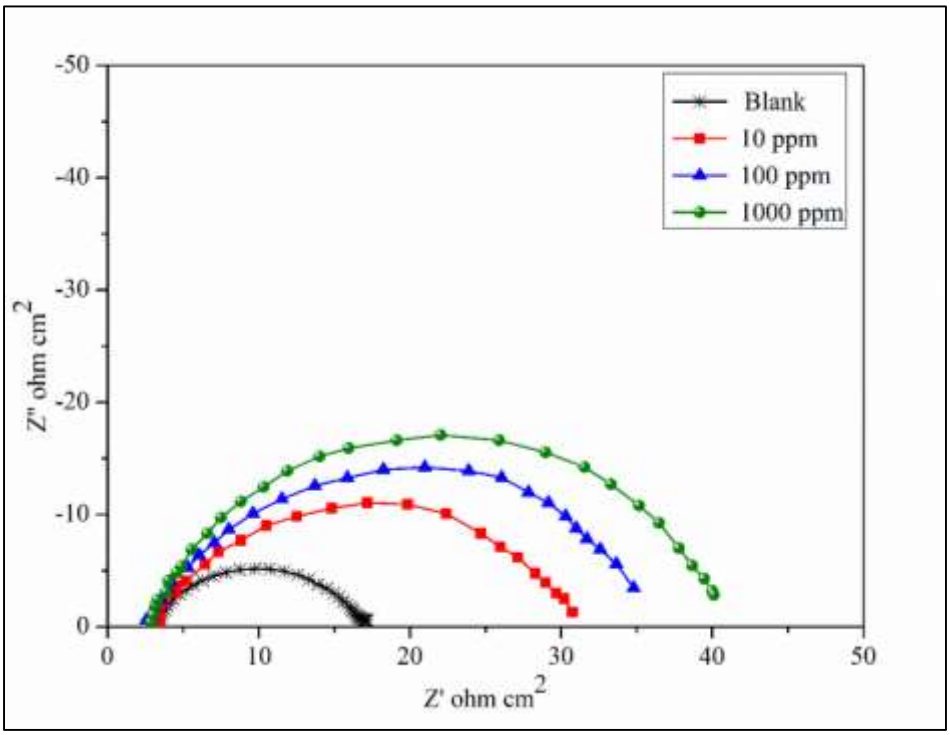

Fig. 3.15 Nyquist plot for mild steel in 0.5 M H_2SO_4 for selected concentrations of PGP

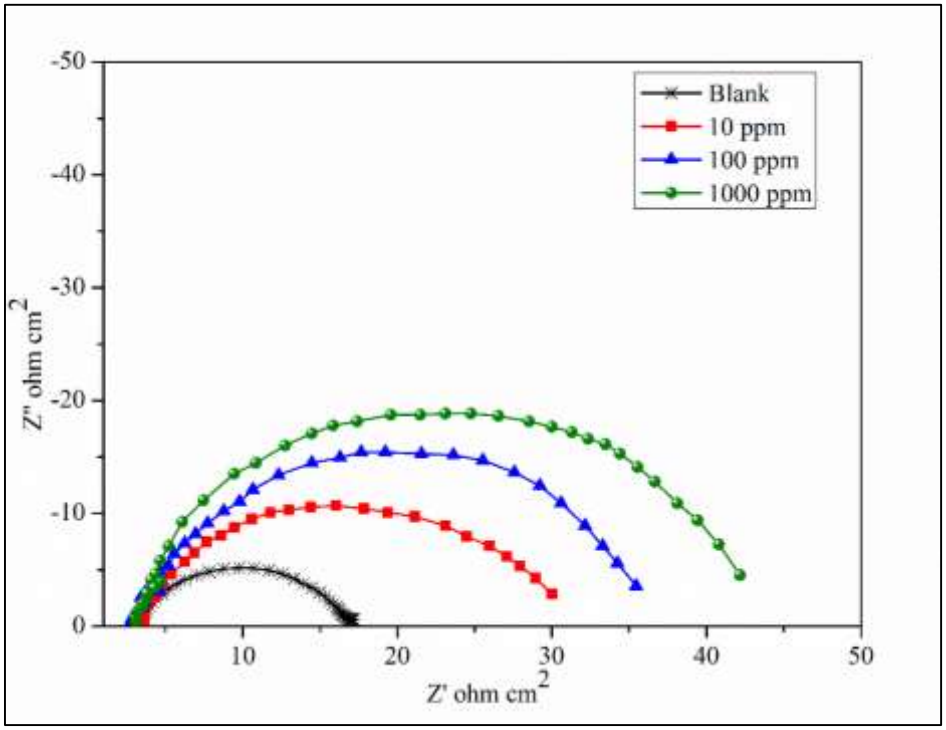

Fig. 3.16 Nyquist plot for mild steel in 0.5 M H_2SO_4 for selected concentrations of PGSU

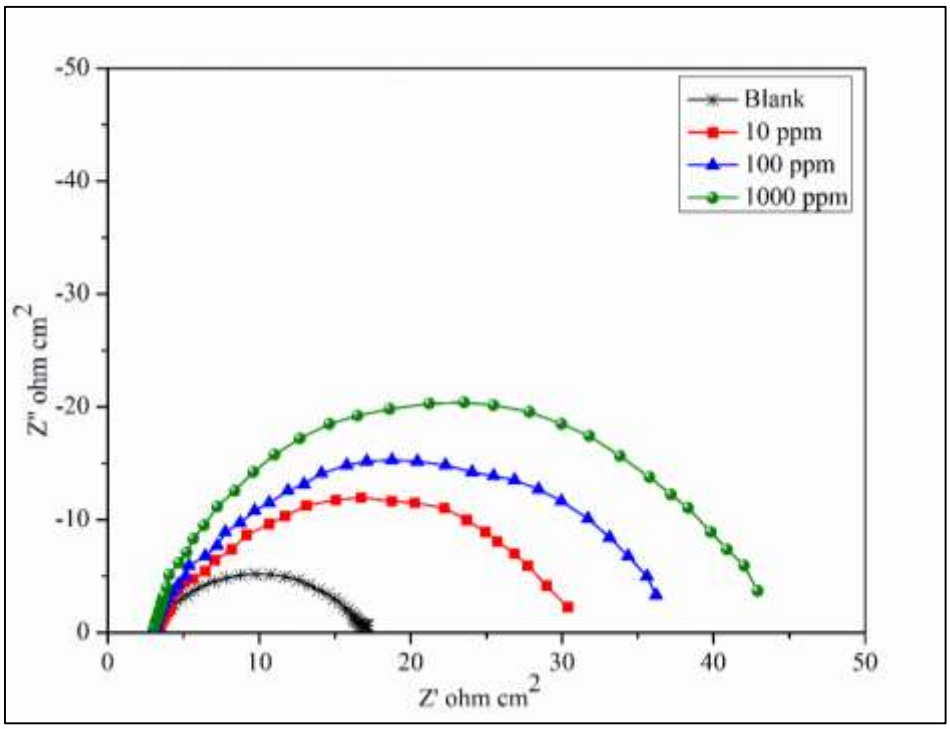

Fig. 3.17 Nyquist plot for mild steel in 0.5 M H_2SO_4 for selected concentrations of PGAZ

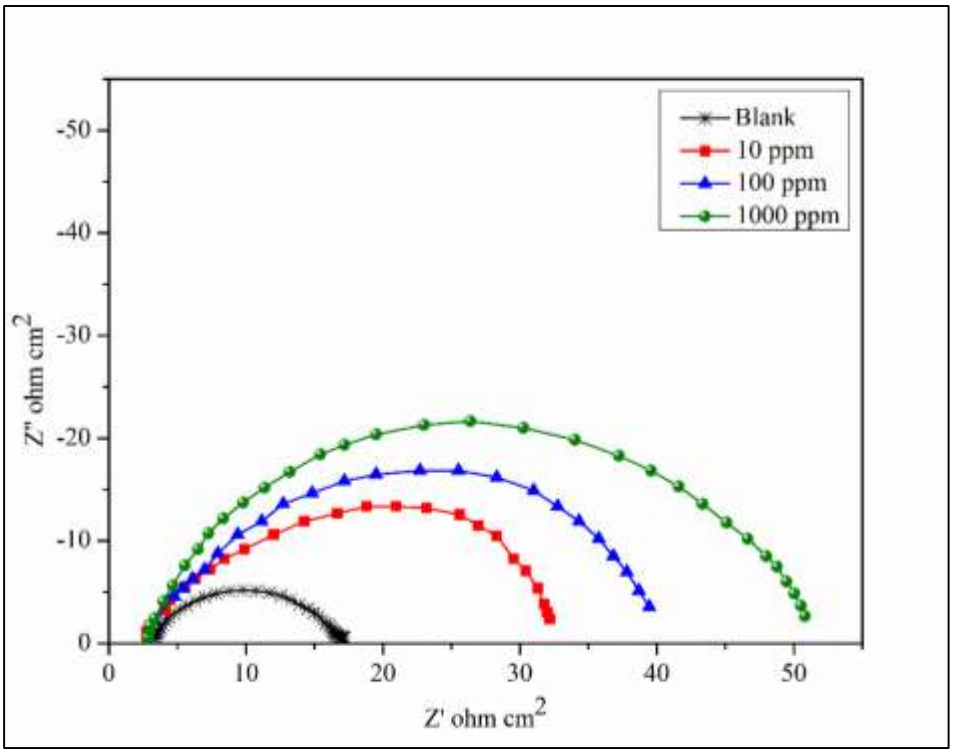

Fig. 3.18 Nyquist plot for mild steel in 0.5 M H_2SO_4 for selected concentrations of PGSE

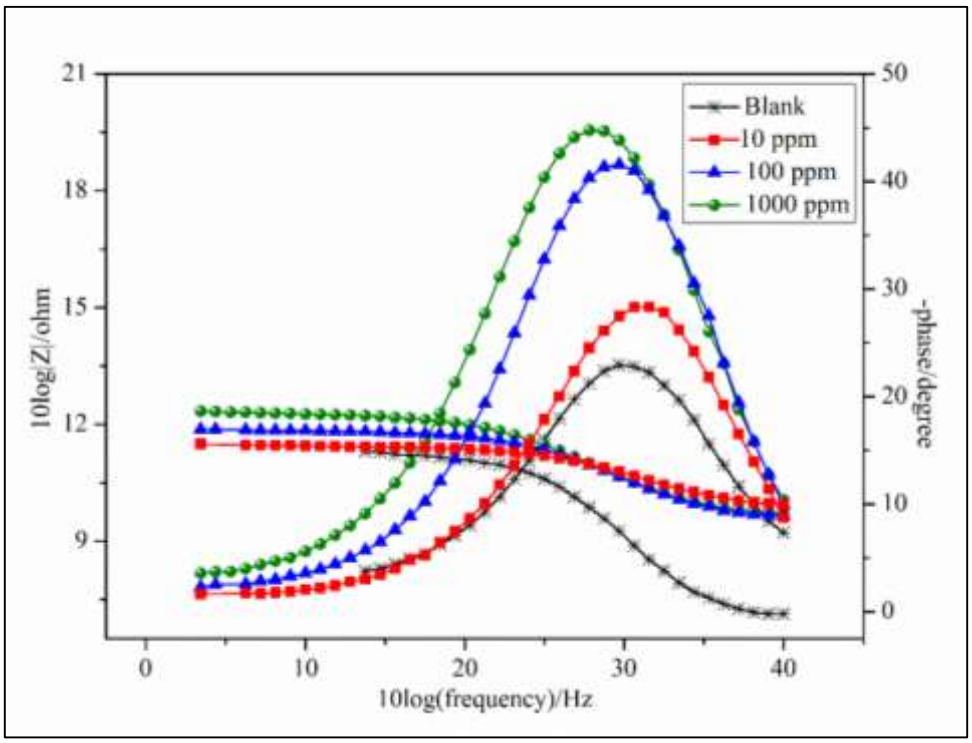

Fig. 3.19 Bode plot for mild steel in 0.5 M H_2SO_4 for selected concentrations of PGM

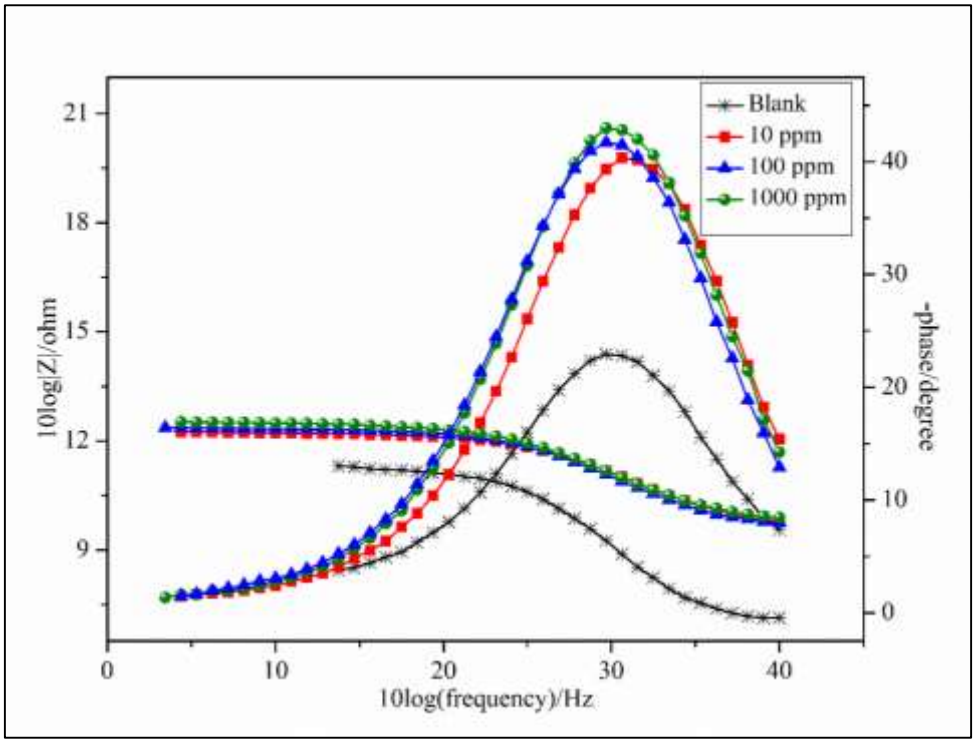

Fig. 3.20 Bode plot for mild steel in 0.5 M H_2SO_4 for selected concentrations of PGS

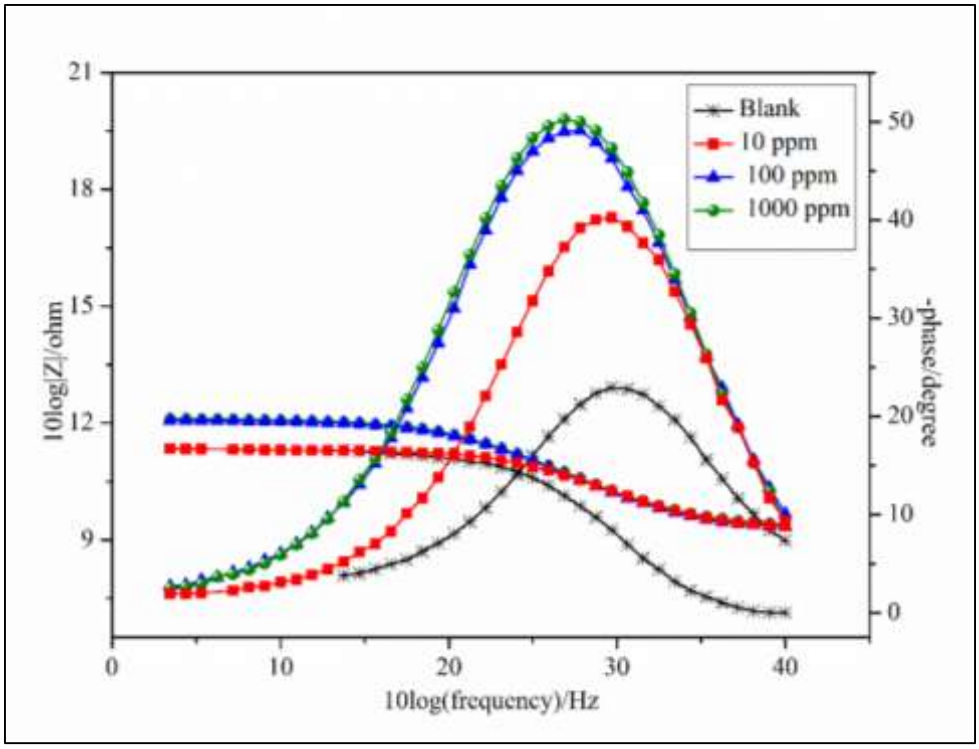

Fig. 3.21 Bode plot for mild steel in 0.5 M H_2SO_4 for selected concentrations of PGG

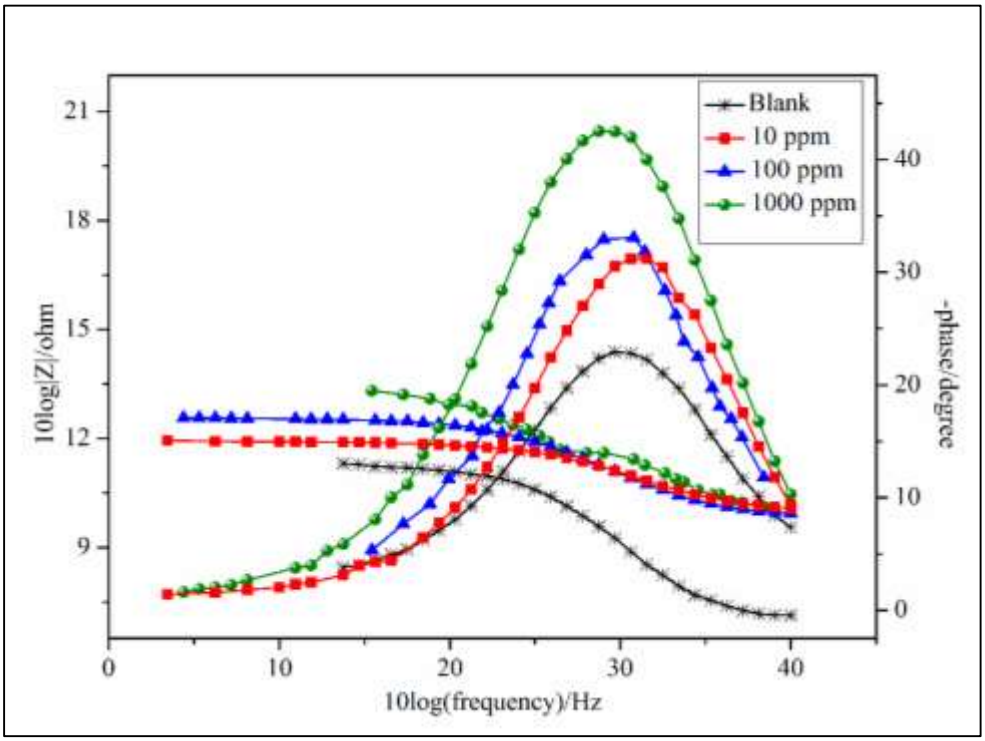

Fig. 3.22 Bode plot for mild steel in 0.5 M H_2SO_4 for selected concentrations of PGA

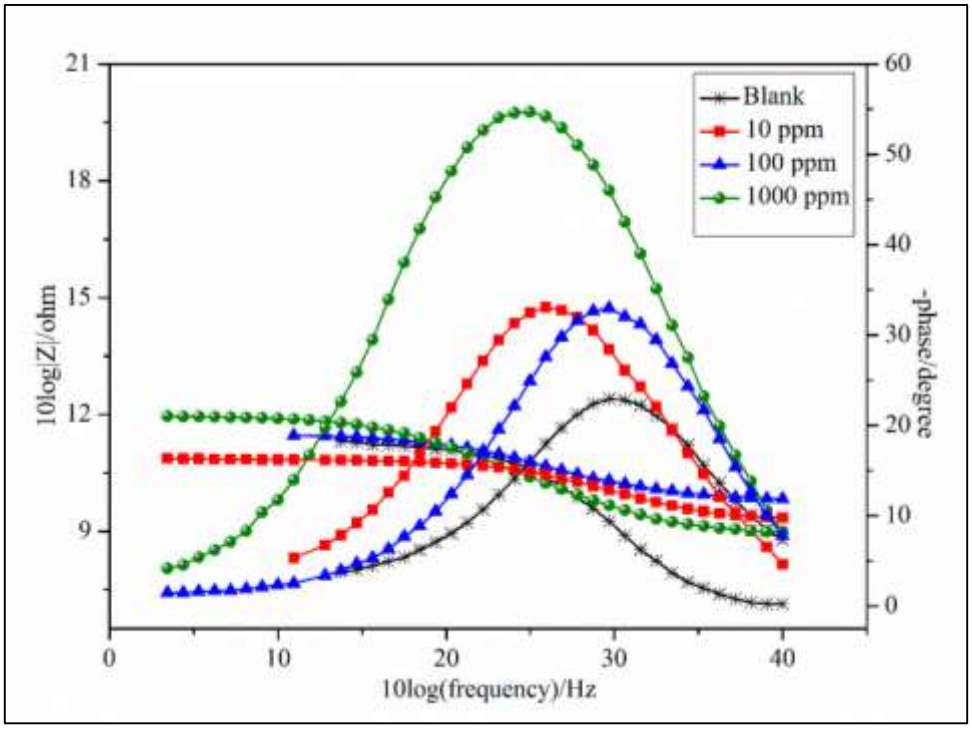

Fig. 3.23 Bode plot for mild steel in 0.5 M H_2SO_4 for selected concentrations of PGP

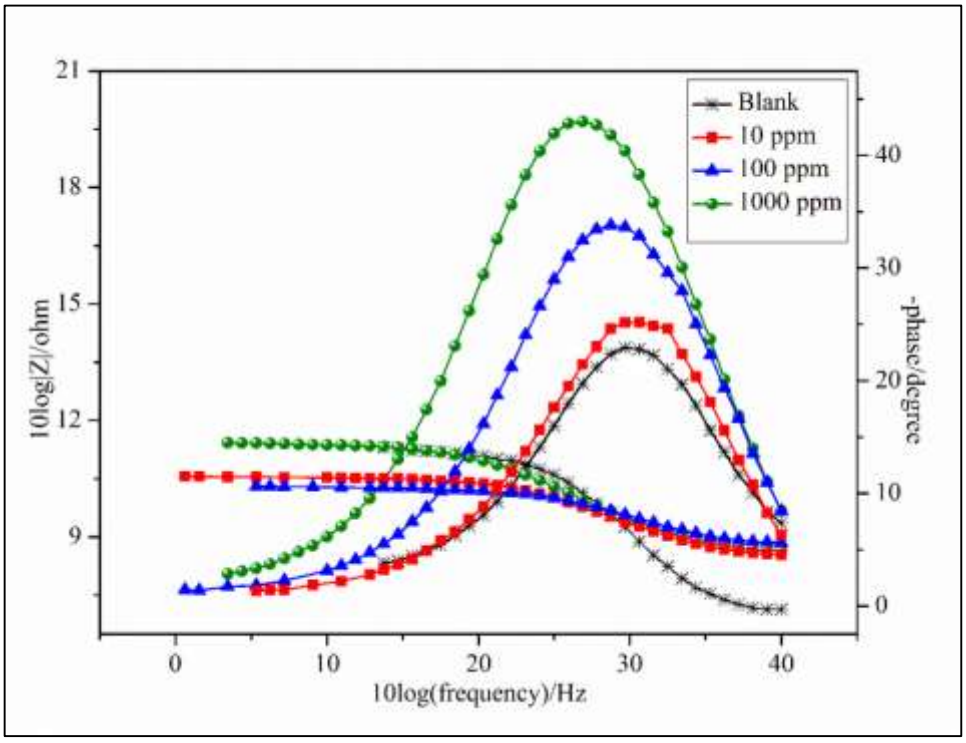

Fig. 3.24 Bode plot for mild steel in 0.5 M H_2SO_4 for selected concentrations of PGSU

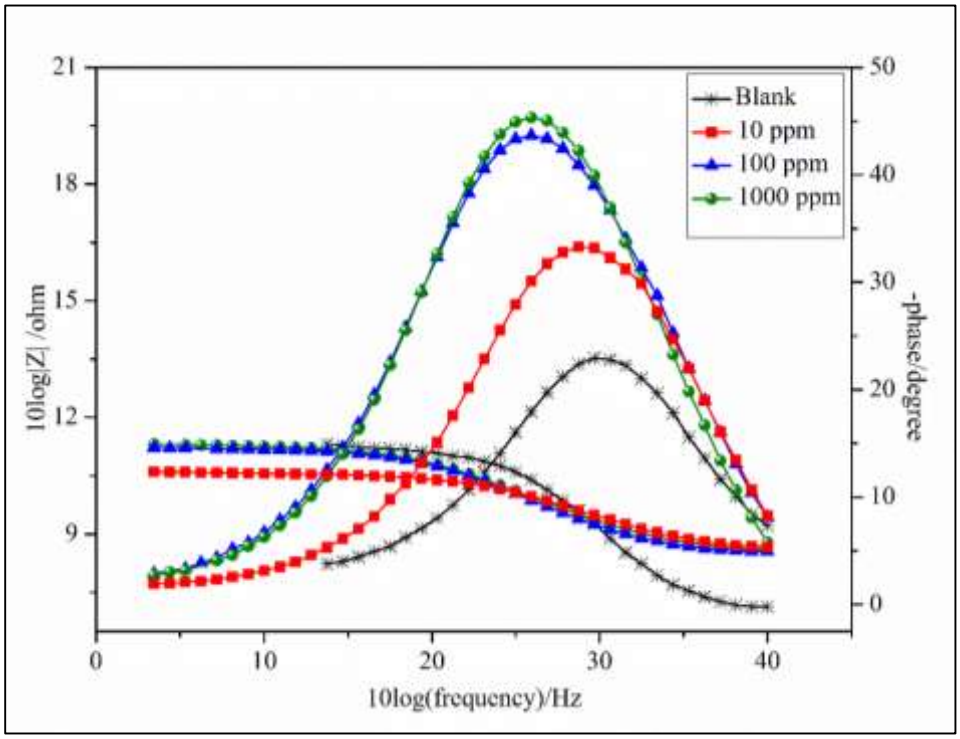

Fig. 3.25 Bode plot for mild steel in 0.5 M H_2SO_4 for selected concentrations of PGAZ

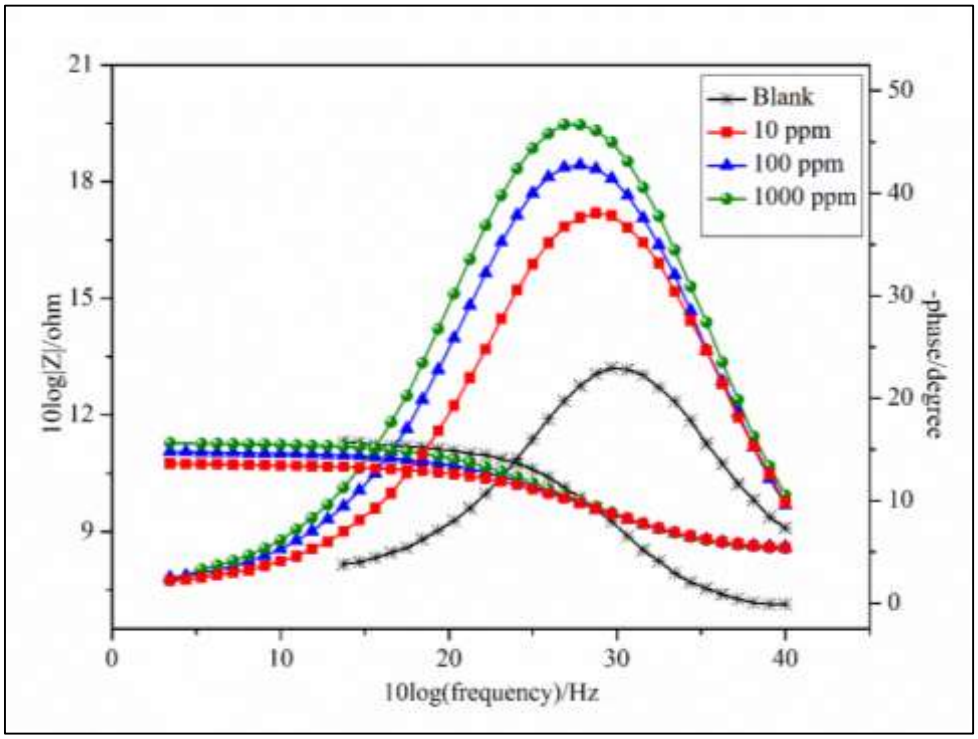

Fig. 3.26 Bode plot for mild steel in 0.5 M H_2SO_4 for selected concentrations of PGSE

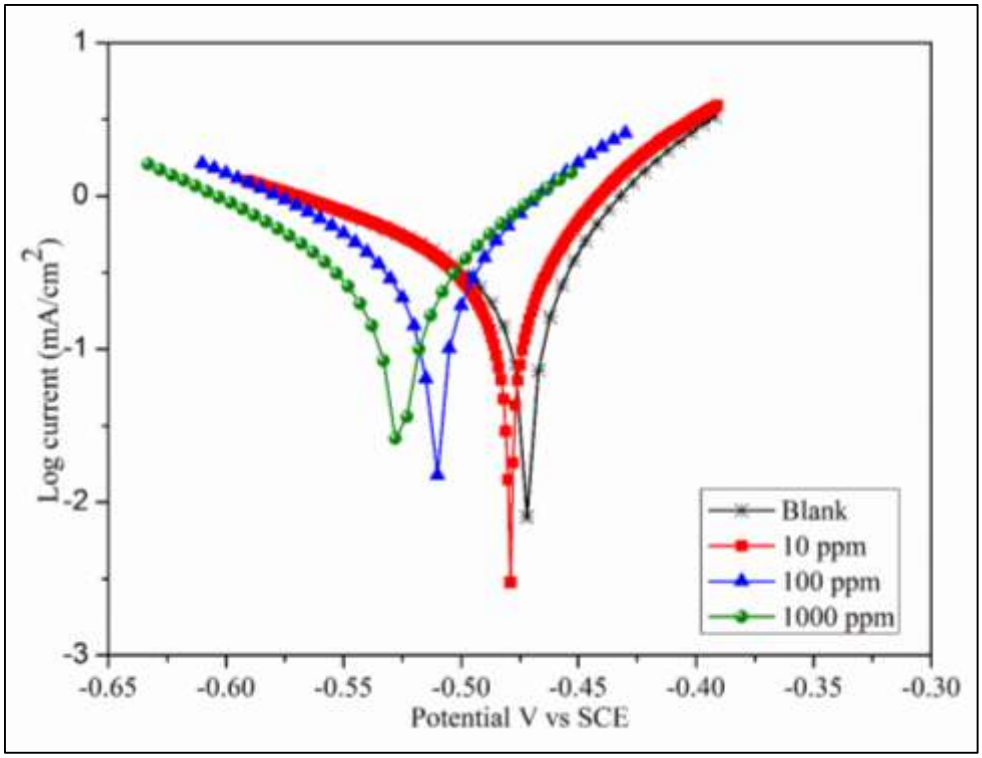

Fig. 3.27 Polarization curves for mild steel in 0.5 M H2SO4 for selected concentrations of PGM

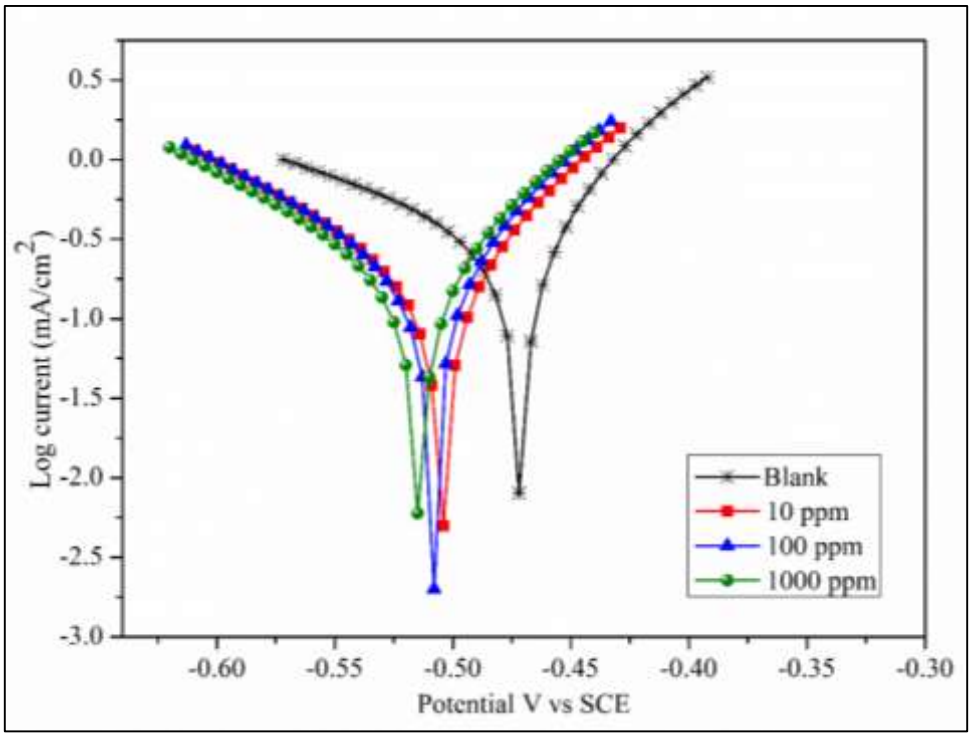

Fig. 3.28 Polarization curves for mild steel in 0.5 M H2SO4 for selected concentrations of PGS

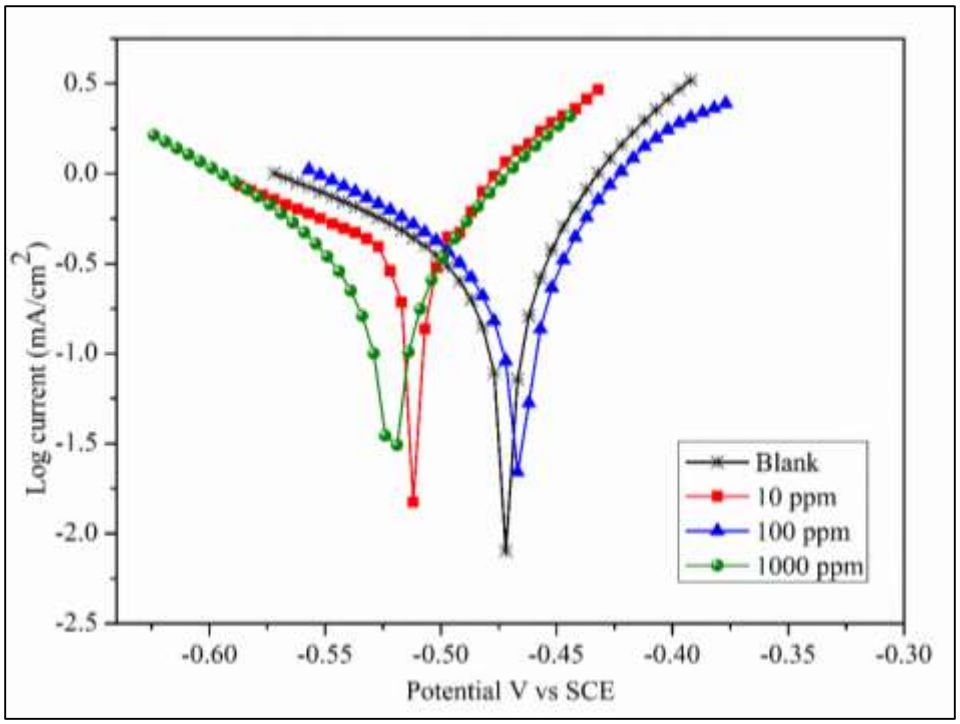

Fig. 3.29 Polarization curves for mild steel in 0.5 M H2SO4 for selected concentrations of PGG

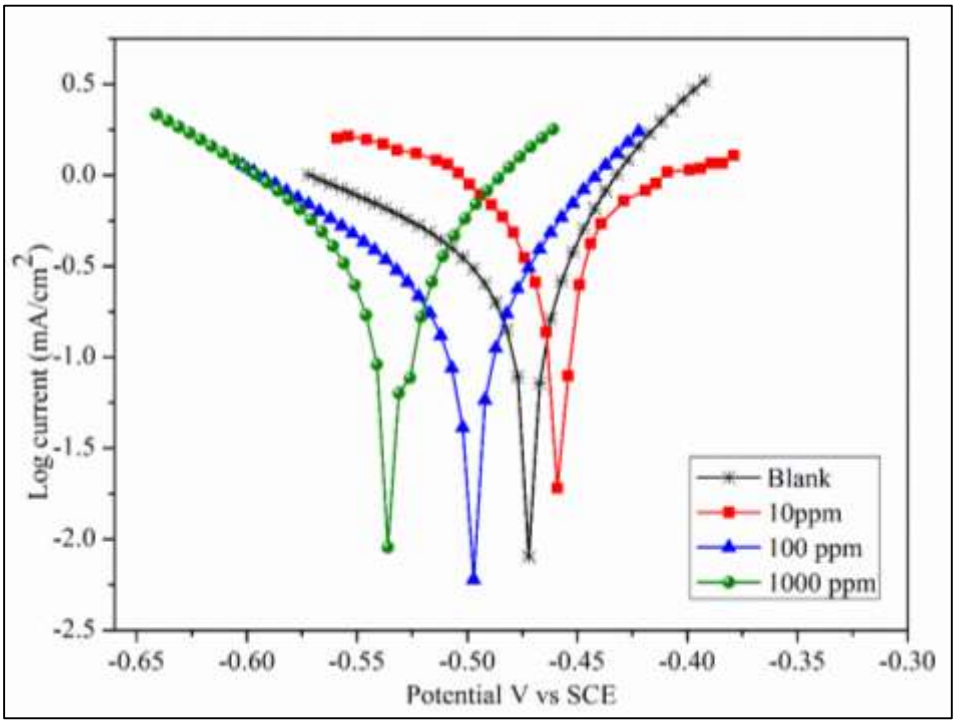

Fig. 3.30 Polarization curves for mild steel in 0.5 M H2SO4 for selected concentrations of PGA

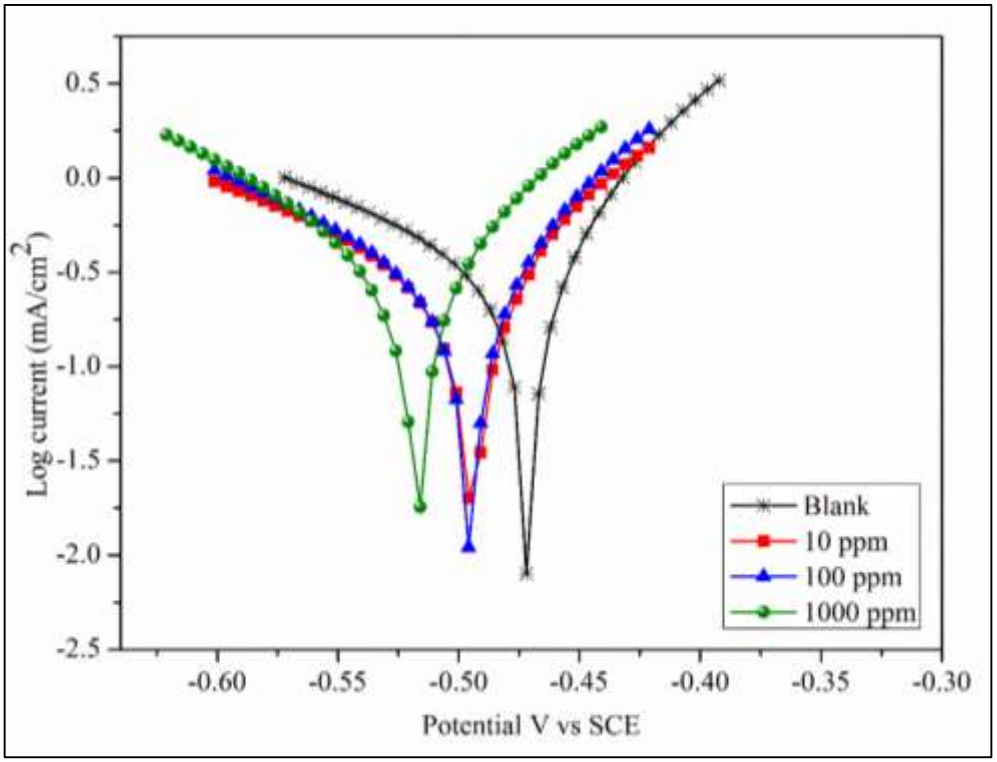

Fig. 3.31 Polarization curves for mild steel in 0.5 M H2SO4 for selected concentrations of PGP

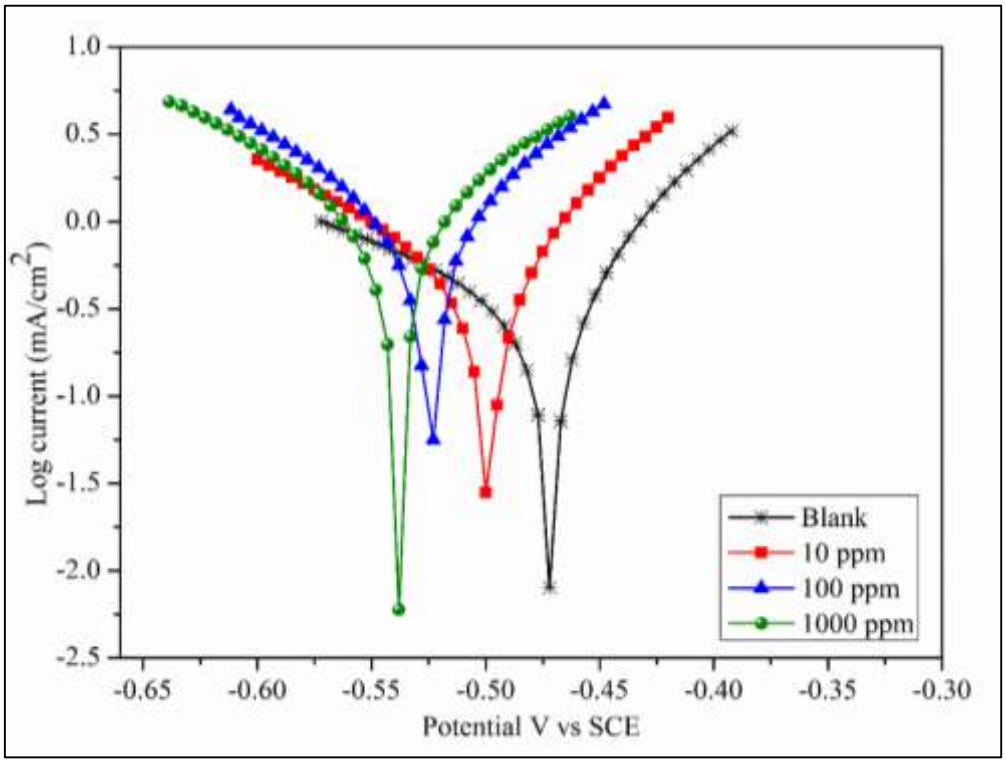

Fig. 3.32 Polarization curves for mild steel in 0.5 M H2SO4 for selected concentrations of PGSU

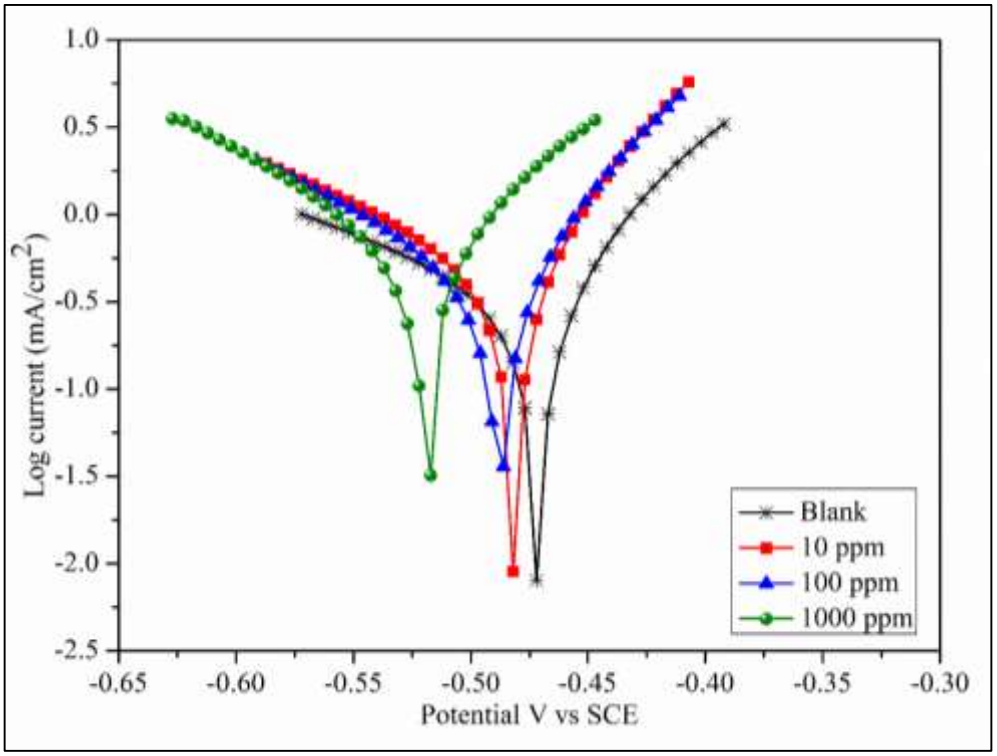

Fig. 3.33 Polarization curves for mild steel in 0.5 M H2SO4 for selected concentrations of PGAZ

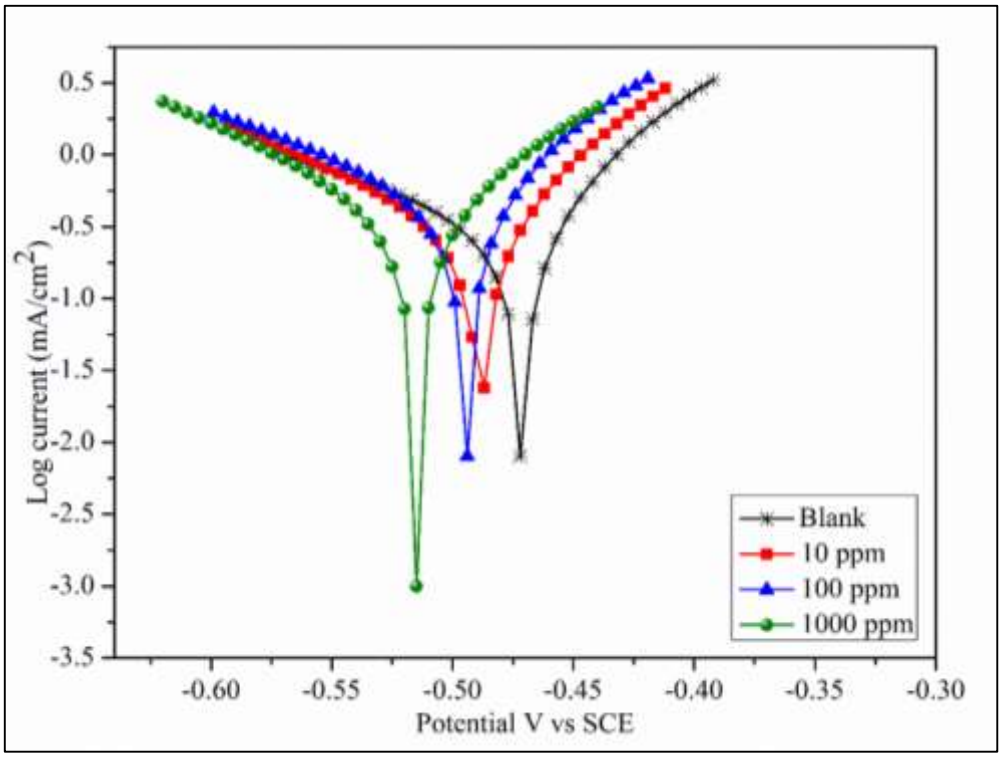

Fig. 3.34 Polarization curves for mild steel in 0.5 M H2SO4 for selected concentrations of PGSE

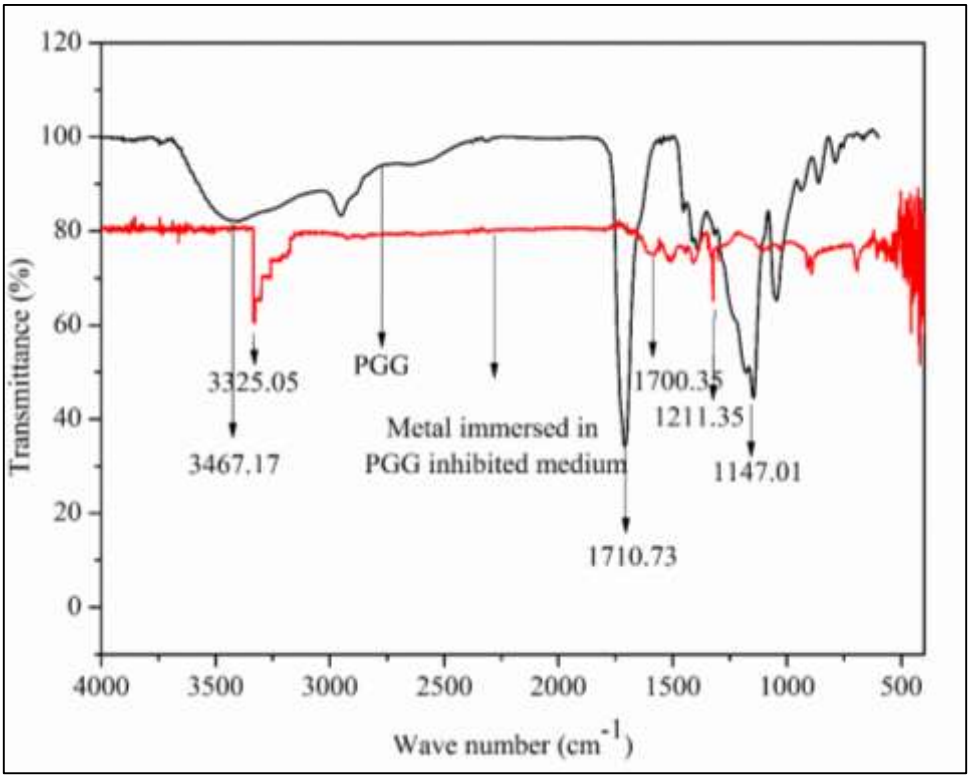

Fig. 3.35 FT-IR spectra of mild steel in PGG and PGG inhibited medium

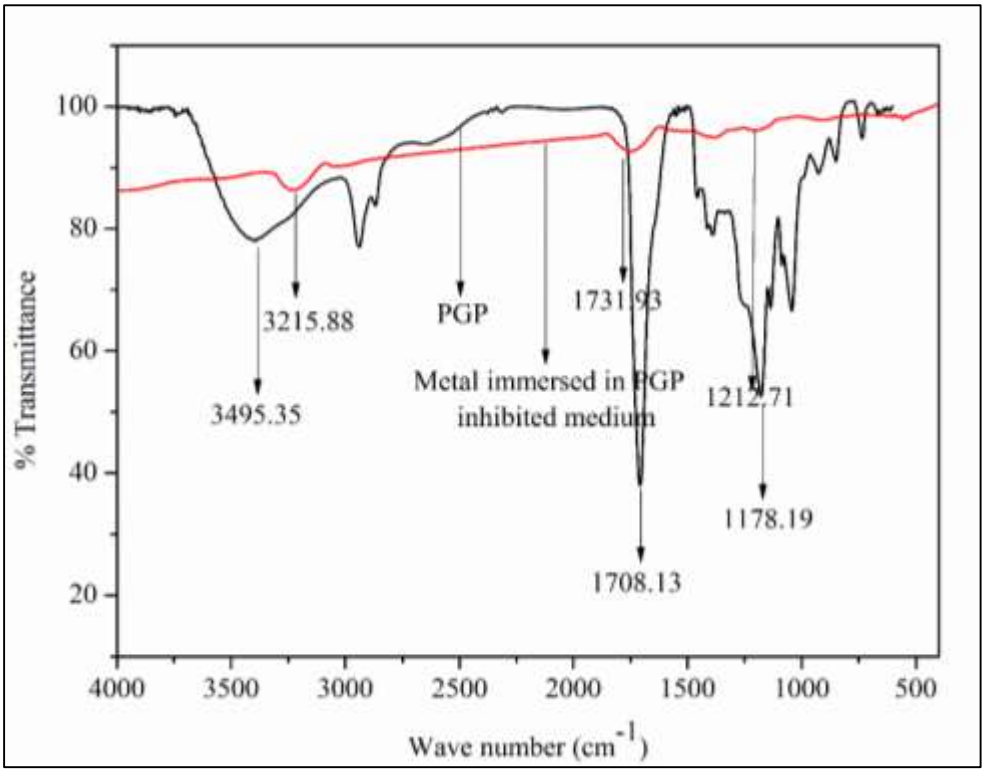

Fig. 3.36 FT-IR spectra of mild steel in PGP and PGP inhibited medium

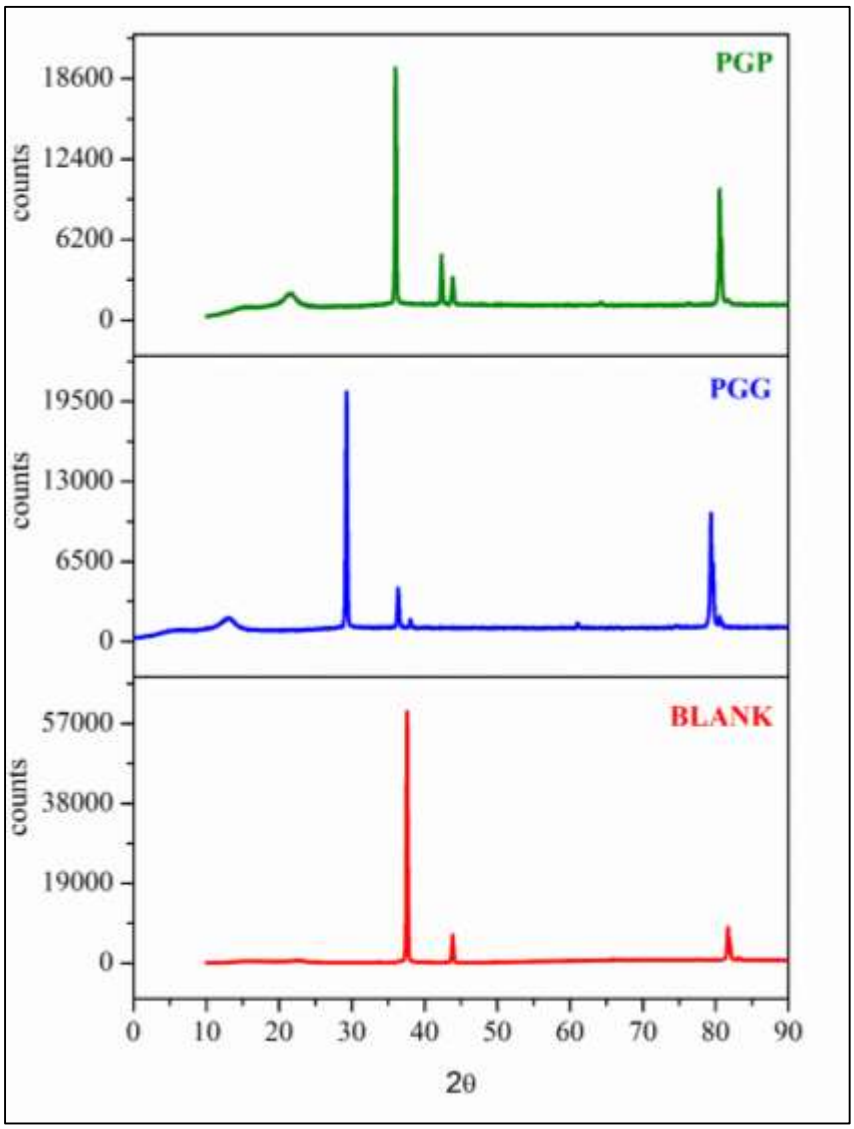

Fig. 3.37 X-ray diffraction patterns of mild steel in uninhibited and inhibited medium

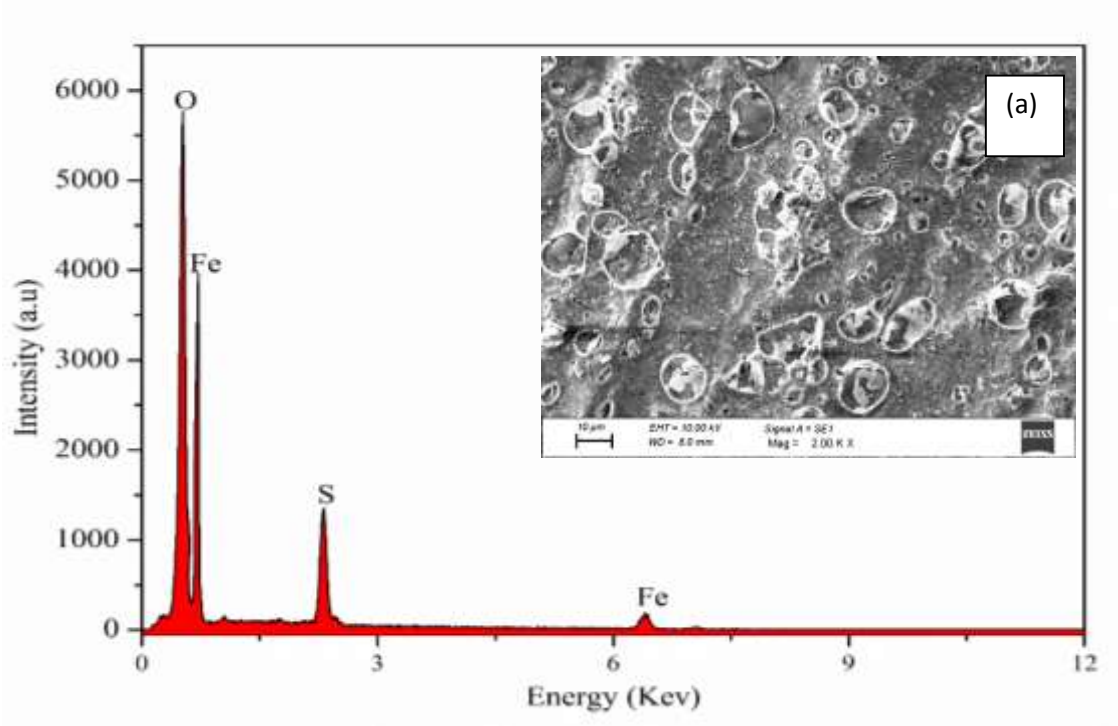
(a)
O
Fe
S
Fe
Intensity (a.u)
Energy (Kev)
0
1000
2000
3000
4000
5000
6000
0
3
6
9
12

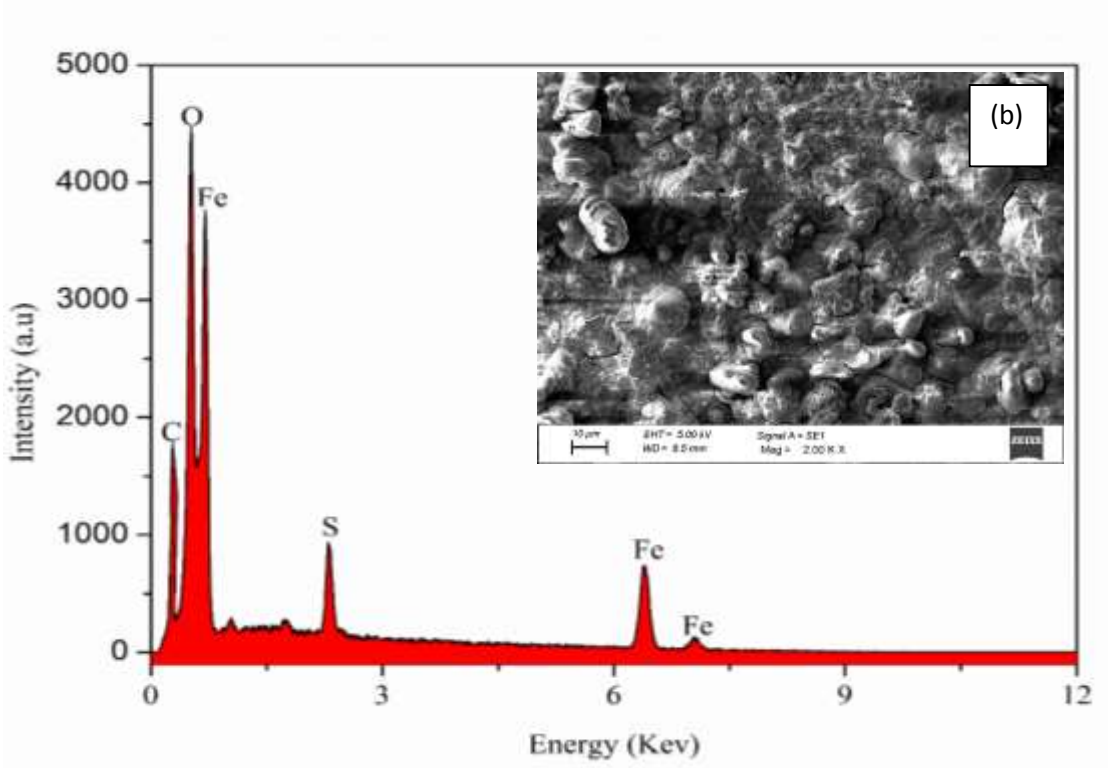
(b)
O
Fe
C
S
Fe
Fe
Intensity (a.u)
Energy (Kev)
0
1000
2000
3000
4000
5000
0
3
6
9
12

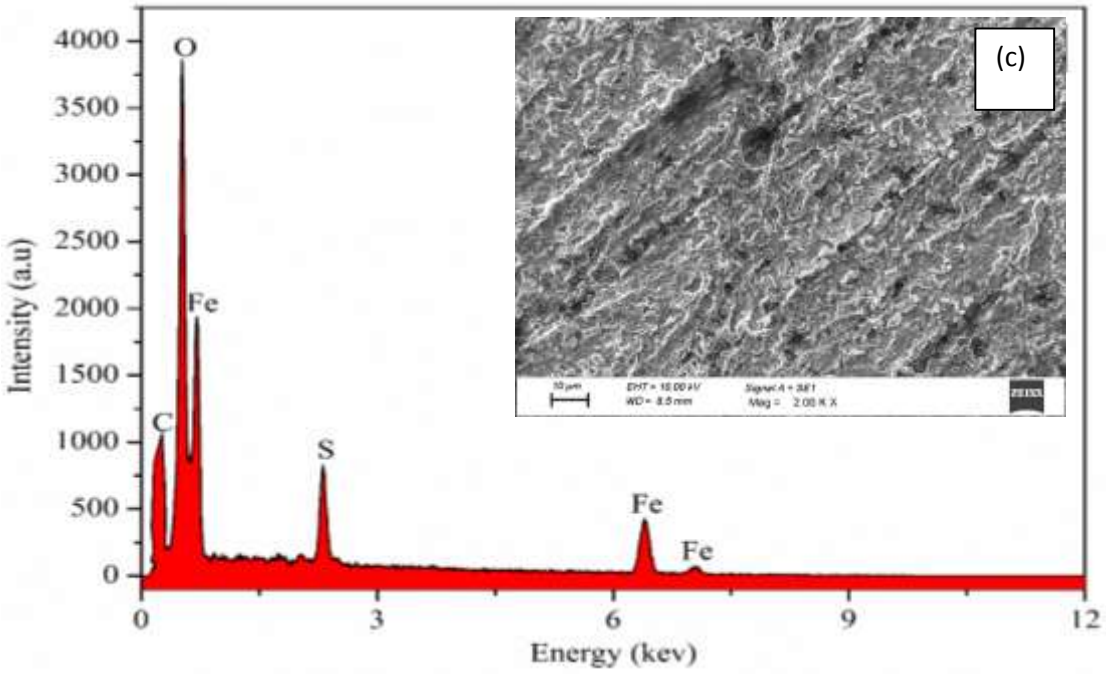

Fig. 3.38 SEM-EDS images of mild steel specimens immersed in (a) 0.5 M H_2SO_4 (b) in presence of PGG (c) in presence of PGP

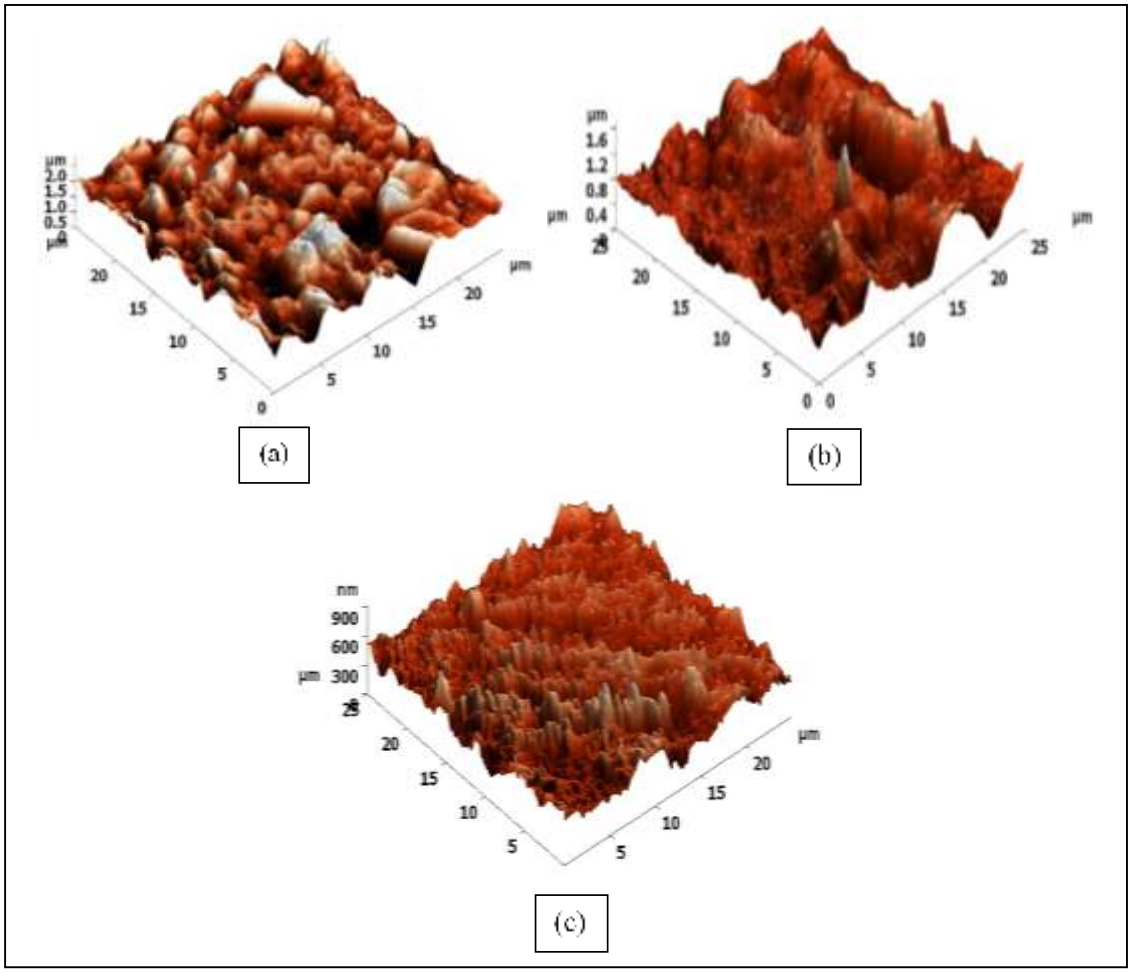

Fig. 3.39 AFM images of mild steel specimens immersed in (a) 0.5 M H_2SO_4

(c) in presence of PGG (c) in presence of PGP

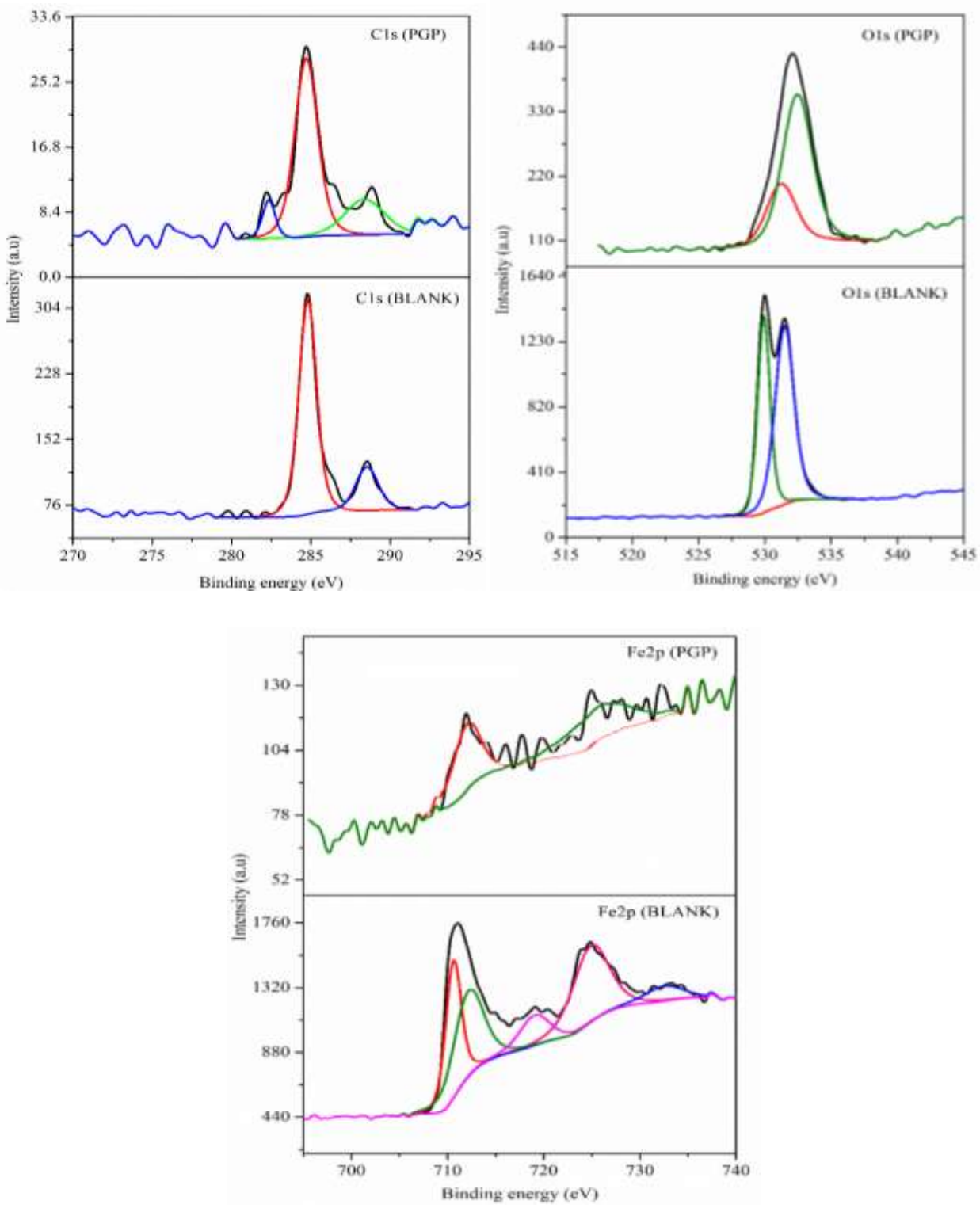

Fig. 3.40 XPS Deconvolution peak of blank and PGP inhibited specimens

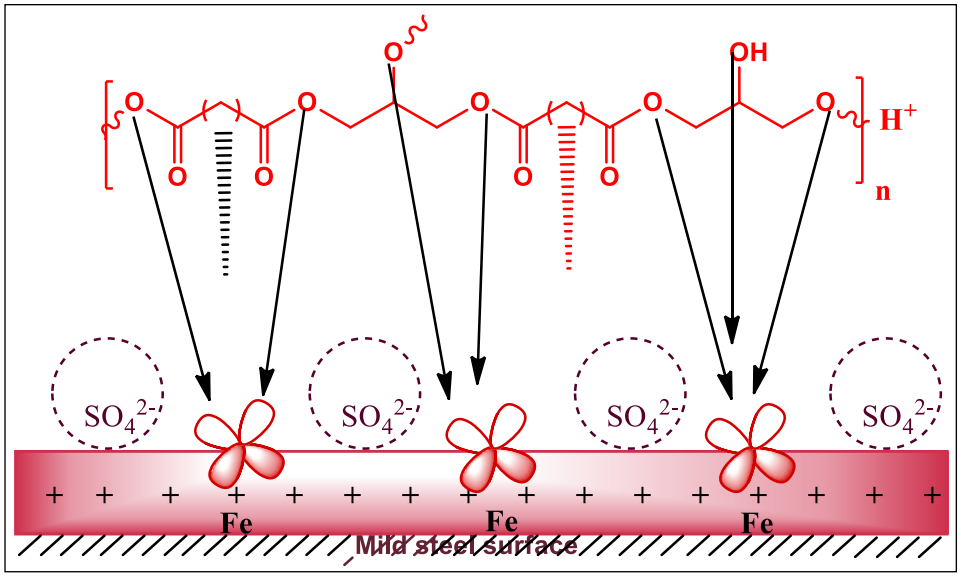

Fig. 3.41 Schematic illustration of the proposed mechanism